Acquisition Algorithm for Continuous Phase Modulation Signal in Walsh Signal Space

by
Kyung-Mi Krystal Park

A Thesis
Submitted to the Faculty of Graduate Studies
in Partial Fulfilment of the Requirements
for the Degree of

Master of Science

Department of Electrical and Computer Engineering
University of Manitoba
Winnipeg, Manitoba
Canada

March, 2004

THE UNIVERSITY OF MANITOBA

FACULTY OF GRADUATE STUDIES
*****
COPYRIGHT PERMISSION

Acquisition Algorithm for Continuous Phase Modulation Signal in Walsh Signal Space

BY

Kyung-Mi Krystal Park

A Thesis/Practicum submitted to the Faculty of Graduate Studies of The University of

Manitoba in partial fulfillment of the requirement of the degree

Of

MASTER OF SCIENCE

Kyung-Mi Krystal Park © 2004

I hereby declare that I am the sole author of this thesis.

I authorize the University of Manitoba to lend this thesis to other institutions or individuals for the purpose of scholarly research.

<div align="center">

K. Krystal Park

</div>

I further authorize the University of Manitoba to reproduce this thesis by photocopying or other means, in total or in part, at the request of other institutions or individuals for the purpose of scholarly research.

<div align="center">

K. Krystal Park

</div>

ACKNOWLEDGMENTS

ABSTRACT

The main attraction of using the CPM receiver in Walsh signal space is its simplicity. Small symbol timing and carrier phase difference between the receiver and received signal can also effectively be synchronized in the steady-state tracking mode.

This thesis focuses on acquiring symbol timing and carrier phase using the Walsh signal space receiver. A pilot signal enables simple and fast acquisition. The acquisition algorithm requires more computation than the steady-state tracking algorithm but there is no added hardware complexity. The acquisition is achieved in a two-step approach by first approximating the carrier phase and symbol timing, and then refining the estimations.

Sending a pilot signal seems like a waste of energy but it is justifiable in overall robustness and for fast acquisition time. Acquisition is achieved with a relatively short training sequence, sometimes as short as 10 symbol bits, with the proposed algorithm that was used.

TABLE OF CONTENTS

LIST OF ABBREVIATIONS

AWGN   Additive White Gaussian Noise

BPSK   Binary Phase Shift Keying

CPM   Continuous Phase Modulation

LRC   L (integer number) Raised Cosine modulation

LREC   L (integer number) RECtangular modulation

MAP   Maximum a Posteriori Probability

MLSD   Maximum Likelihood Sequence Detection

MLSE   Maximum Likelihood Sequence Estimation

MSK   Minimum Shift Keying

m-PSK   M-ary Phase Shift Keying

PM   Phase Modulation

PSK   Phase Shift Keying

QPSK   Quadrature Phase Shift Keying

RMS   Root Mean Square

SNR   Signal to Noise Ratio

TDMA   Time Division Multiple Access

LIST OF FIGURES

LIST OF TABLES

INTRODUCTION

Digital communication has such overwhelming advantages over analog that it increasingly dominates communication systems [LeMe94]. Though, computer to computer communication is inherently digital, even analog signals such as voice and other biological signals are being converted to digital format. Advantages of digital communication include reduced bandwidth and greater overall system capacity. It is, however, susceptible to errors. Generally, various coding and modulation schemes are used as error combating techniques.

Continuous phase modulation (CPM) is particularly attractive in this regard because its memory serves as a coding without introducing redundant symbols. CPM also has good power and bandwidth efficiency compared to other modulation and coding techniques. Finally, it generates constant envelope waveforms that are attractive in applications involving nonlinear amplifiers [GiMM99].

The major drawback of CPM is that the optimum receiver has typically a large bank of matched filters followed by a trellis decoder [AnAS86]. Therefore, considerable research has focused on finding a simplified CPM receiver: by reducing the number of filter banks [Kram92], by representing CPM as a superposition of simpler waveforms

[Laur85, MeMo85], or by projecting CPM into different signal spaces [Tang98, TaSh00]. Other research has sought to simplify the trellis [Seve91, Lars90].

This thesis considers the receiver which projects CPM to the Walsh signal space [Tang98]. Typically the receiver is assumed to be coherent which requires complete knowledge of the transmission carrier and symbol timing. Thus, either the carrier phase and symbol timing must be precisely known or a reasonably accurate synchronization must be established before this receiver can be used. Phase and time acquisition techniques for CPM receivers based on the Walsh signal space are the major focus of the research in this thesis.

This chapter briefly introduces digital communication systems and presents the mathematical background of CPM. Research objectives and the outline of the overall thesis are provided at the end of the chapter.

1.1 Digital Communication System

In digital communication, the information is sent by a data sequence **a**, a sequence of symbols which is from either an M-ary or binary alphabet. Typically to combat error, the signal is encoded by mapping k information symbols into n channel symbols before modulation. Thus, n-k redundant symbols are used for error control. However, this type of coding is not discussed in this thesis. After coding, the coded bits are digitally modulated to accommodate the channel. A communication channel is the physical medium that is used to send a signal from the transmitter to the receiver. In wireless communication the medium is air, while a telephone channel employs a variety of

physical media. Regardless of the media, the transmitted signal, $x(t)$, is corrupted in a random manner by a variety of possible mechanisms, such as additive thermal noise generated by electrical devices, man-made noise such as automobile ignition and atmospheric noise such as electrical lightening during a thunderstorm. After the signal has passed through the channel, the corrupted received signal $r(t)$ can be written as

$$r(t) = \alpha \ x(t) + n(t) \tag{1-1}$$

where, $n(t)$ represents the additive noise and α represents the attenuation factor. The most common corruption is a thermal noise which is generally characterized as Additive White Gaussian Noise (AWGN) with power spectrum density $N_0/2$ (Watts/Hz) where N_O varies in different channels. This is the noise model used in this thesis, with the noise denoted as $w(t)$.

A general model for the digital communication system is shown in the following figure.
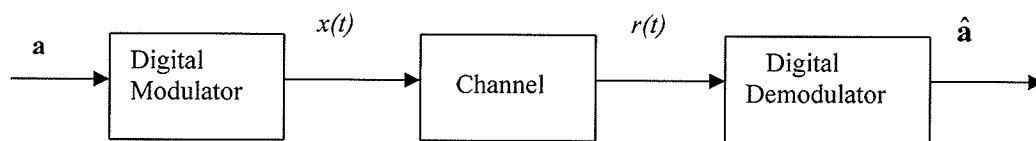
Figure 1.1 The digital communication system model.

Usually, the power and bandwidth efficiency as well as the accuracy of the recovered signal determine the performance of the modulation scheme. Generally, the Signal to Noise Ratio (SNR) is the key factor in improving the accuracy of the detection. SNR can be improved by increasing the power but SNR is subject to the physical

limitation of the equipment and to cost limitation. Although power efficiency and bandwidth efficiency are usually contradictory requirements, CPM is a modulation method that is both more bandwidth and power efficient than its predecessors.

1.2 Digital Phase Modulation

Digital phase modulation (PM) has a constant envelope, a property that is attractive in many communication systems. In PM, the information is carried in phase of the signal. The following equation expresses PM

$$x(t) = \sqrt{\frac{2E}{T}} \cos(2\pi f_c t + \varphi(\mathbf{a}, t)) \qquad (1\text{-}2)$$

where f_c is the carrier frequency, T is the length of a symbol time interval; E is the energy expended during the period T and $\mathbf{a}$ is the M-ary data sequence from M-ary alphabet, $\{0,1,\ldots(M\text{-}1)\}$. If the information phase $\varphi(\mathbf{a}, t)$ is defined as

$$\varphi(\mathbf{a}, t) = \frac{2\pi}{M} a_n \qquad (1\text{-}3)$$

for n_{th} interval, [nT, (n+1)T) when $a_n \in \{0,1,\ldots(M\text{-}1)\}$ is the data symbol, one has the special digital phase modulation called Phase Shift Keying (PSK). When M=2, it is called Binary Phase Shift Keying (BPSK) and when M=4, it is called Quadrature Phase Shift Keying (QPSK) (see Figure 1.2). PSK is an attractive modulation method because it employs rather simple techniques both for the modulation and demodulation while offering constant envelopes and power efficiency. Generally, f_c is much larger then $1/T$

but in the Figure 1.2 f_c is set equal to $1/T$ to clearly show the discontinuities in the

modulated signal.
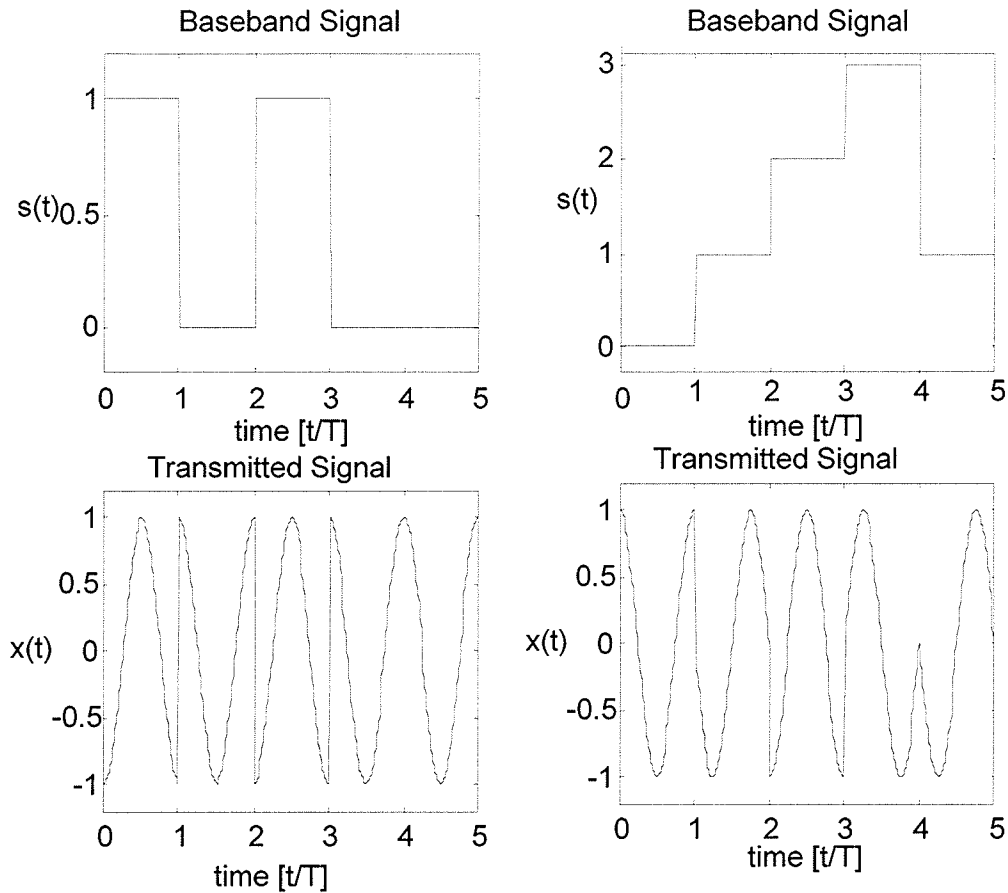
Figure 1.2 PSK and QPSK Signal

Though PSK is relatively power efficient, it has poor bandwidth efficiency

because of the discontinuities at the interval boundaries as seen clearly in Figure 1.2. The

maximum derivative of the signal determines the bandwidth and whenever there are

discontinuities the maximum derivative goes to infinity. To examine this problem more

closely rewrite equation (1-2), using equation (1-3),

$$x(t) = \sqrt{\frac{2E}{T}} \left[\mu(t - nT) \cos\left(\frac{2\pi}{M} a_n\right) \cos(2\pi f_c t) - \mu(t - nT) \sin\left(\frac{2\pi}{M} a_n\right) \sin(2\pi f_c t) \right] \quad (1\text{-}4)$$

where, $\mu(t)$ is called a shaping pulse.

For BPSK or QPSK (or in general m-PSK), it is defined as:

$$\mu(t) = \begin{cases} 1 & 0 \leq t < T \\ 0 & \text{otherwise} \end{cases} \qquad (1\text{-}5)$$

Clearly, the discontinuity lies within the shaping pulse. Thus, one can reduce the bandwidth by changing the shaping pulse to be wider and/or to be continuous. However, making the shaping function wider causes inter-symbol interference and changing the rectangular shaping function into other shapes causes the constant envelope to be distorted.

1.3 Continuous Phase Modulation

Continuous Phase Modulation (CPM) was introduced to make symbol boundaries continuous while keeping the envelope constant.

The discontinuity comes from the shaping pulse as can be seen from equation (1-4). Changing the shaping pulse $\mu(t - nT)$ will cause inter-symbol interference. Thus, instead of using the shaping pulse to change the envelope of the modulated signal (hence, minimize the discontinuity), a phase smoothing function can be used to reduce the discontinuity. Furthermore, memory could be introduced in the phase to create a coding effect.

To see how this is accomplished, rewrite Equation (1.2) in complex notation

$$x(\mathbf{a}_n, t) = \text{Re}\{s(\mathbf{a}_n, t) \exp(j2\pi f_c t)\} \qquad (1\text{-}6)$$

where,

$$s(\mathbf{a}_n, t) = \sqrt{\frac{2E}{T}} \exp(j\varphi(\mathbf{a}_n, t)) \qquad (1\text{-}7)$$

is the complex envelope of the transmitted signal $x(\mathbf{a}_n, t)$ relative to frequency f_c; E is the

energy per symbol; T is the length of symbol interval; $\mathbf{a} = (\ldots, a_{-1}, a_0, a_1, \ldots)$ is the

transmitted data sequence with $a_i \in \{\pm 1, \pm 3, \ldots, \pm(M-1)\}$. The phase $\varphi(\mathbf{a}_n, t)$ with

$\mathbf{a}_n \equiv (\ldots a_{n-1}, a_n)$ bears the information which is written as

$$\varphi(\mathbf{a}_n, t) = 2\pi \sum_{i=-\infty}^{n} h_i a_i q(t - iT) \qquad\qquad nT \le t < (n+1)T. \qquad (1\text{-}8)$$

It can be seen from the above equation that the phase, $\varphi(\mathbf{a}_n, t)$, is determined by

all the bit information up to n_{th} bit information. In equation (1-8) h_i is the modulation

index and takes value from the set $\{h_o, h_1, \ldots, h_{H-1}\}$ cyclically. Although, h_i can be any

number, for practical reasons it is a rational number less than 1. For H=1, the scheme is

called a *single-h* and for H>1, it is called *multi-h* where H is a small integer. *Multi-h* is

known to be an effective approach to increase the power efficiency over *single-h*; the

price paid is the added complexity of the receiver. $q(t)$ is the phase smoothing function

which is also called a phase pulse.

The phase pulse, $q(t)$ is restricted as follows:

$$q(t) = \begin{cases} 0 & t \le 0 \\ 1/2 & t \ge LT \end{cases} \qquad (1\text{-}9)$$

To have a continuous phase, $q(t)$ just has to be a continuous function. However, to

increase the bandwidth efficiency, $q(t)$ should have the smallest maximum derivative

possible. Furthermore, a $q(t)$ which has more higher derivatives before encountering an

impulse is known to be more bandwidth efficient. Two common examples of $q(t)$ are

LRC and LREC.   If L=1, it is called full response and if L>1 it is known as a partial

response. Partial response is one way to reduce the bandwidth requirement but it is not as

power efficient as the full response system. LREC and LRC are described by the

following equations with plots of them shown in Figure 1.3.

LREC:

$$q(t) = \begin{cases} 0 & t \leq 0 \\ t/2LT & 0 \leq t < LT \\ 1/2 & t \geq LT \end{cases} \tag{1-10}$$

LRC:

$$q(t) = \begin{cases} 0 & t \leq 0 \\ \dfrac{1}{2}\left[\dfrac{t}{LT} - \dfrac{1}{2\pi}\sin\dfrac{2\pi}{LT}t\right] & 0 \leq t < LT \\ 1/2 & t \geq LT \end{cases} \tag{1-11}$$

It can be seen from the equation (1-11) and the plot of Figure 1.3, that partial response

(L>1) will have a smaller maximum derivative and that LRC can be differentiated more

times than LREC before an impulse function occurs.
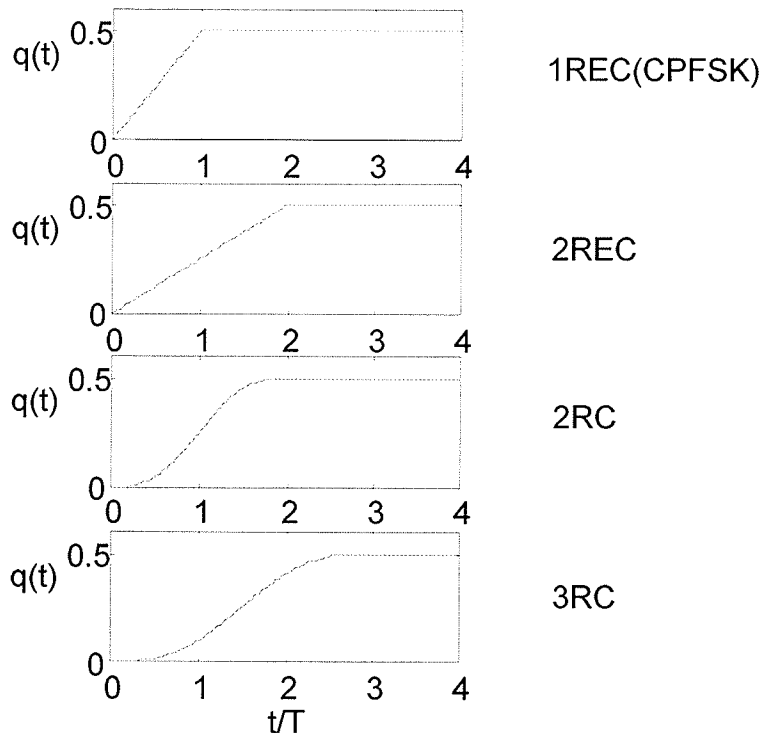
Figure1.3 Examples of LREC and LRC CPM phase pulses.

1.4 Objectives of the Study

CPM has been the focus of much research interest because of the many attractive

features such as high efficiency in power and bandwidth. Despite this, its current usage

is limited to simple schemes such as MSK (Minimum Shift Keying) only. The reason for

its limited usage always has been the complexity of the demodulation and the receiver

design. Considerable research has been dedicated to finding a simplified solution for the

receiver design.   A typical coherent receiver requires reasonably accurate

synchronization. Tang's research [Tang98] focused on the steady-state tracking aspect of

the synchronization using Walsh signal space. In the steady-state tracking mode it is

assumed that reasonably reliable clock, carrier and data value have been established. The synchronizer then needs only to track small changes caused by channel and/or the transmitter drift, and to combat noise.

This thesis is an attempt to broaden Tang's synchronization technique to the acquisition mode which occurs when the receiver is first turned on. During the acquisition-state the synchronizer needs to be locked on to the symbol clock and carrier. The symbol and carrier frequency is rather easy to obtain and assumed to be known. This thesis focuses on acquiring symbol timing and carrier phase using the Walsh signal space receiver.

1.5 Outline of the Thesis

In Chapter 2, the basics of the optimum CPM receiver, as well as the sub-optimum receivers using a different signal space are discussed. Also, this chapter introduces the trellis and Viterbi algorithm. Next, Walsh functions are introduced and the advantage of using Walsh signal based CPM receiver structure. Chapter 3 deals with data-aided bit time and carrier phase acquisition techniques. Performance evaluation of acquisition of the time and phase error is given in Chapter 4. The minimum length of training signal and the signal requirements are discussed. Finally, the conclusion and suggestions for further research are presented in Chapter 5.

CPM RECEIVERS

Although, there are two basic types of receivers, a coherent and non-coherent type, only the coherent type is discussed because the non-coherent receiver has poor performance for CPM.

A typical optimum receiver has a bank of matched filters to generate the sufficient statistics, followed by a trellis decoder. The trellis decoding depends on the criterion used. Two common ones are MAP (maximum a posteriori probability) symbol detection where the decision is made on a symbol-by-symbol basis, with each symbol decision based on an observation of received data sequence and MLSD (Maximum Likelihood Sequence Detection). MLSD is more commonly known as MLSE (Maximum Likelihood Sequence Estimation). Both, MAP and MLSD can be used to decode a signal with memory, but the only the simpler one, MLSD, is discussed in this thesis. In general, the optimum receiver, in MLSD sense, for CPM is not practical because of its complexity in receiver design, in particular, a large matched filter bank. This chapter provides the basic concepts behind optimum and simplified sub-optimum receivers.

2.1 MLSD Receiver for CPM in an AWGN Channel

The received signal, corrupted by noise, can be written in the baseband as

$$r(t) = s(t) + w_R(t) + jw_I(t) \tag{2-1}$$

where the noise is Gaussian and has independent real and imaginary components, $w_R(t)$, and $w_I(t)$, each with spectral density of No/2 and the signal is

$$s(t) = \sqrt{\frac{2E_s}{T}} \exp[j(\theta + \varphi \ (\mathbf{a}; t - \tau \ ))]. \tag{2-2}$$

θ and τ are carrier phase and time uncertainty in the received signal and $\mathbf{a}$ is the data sequence. It is assumed that the receiver knows the carrier frequency f_c and symbol period T. To determine the likelihood function, discretize the waveform by sampling $r(t)$ every T_s seconds. The samples, $r(k)$, are

$$r(k) = \sqrt{\frac{2E_s}{T}} \exp[j(\theta + \varphi \ (\mathbf{a}; kT_s - \tau \ ))] + w_R(k) + jw_I(k) \quad k = 0,1,2,.... \tag{2-3}$$

where, $w_R(k)$ and $w_I(k)$ have the same variance $\sigma_n^2 = (N_o / 2)/T_s$. Over the time interval corresponding to N symbols, sequence $r(k)$ has $N \times L_O$ elements, where L_O is T/T_s. This set of sample is used to express the likelihood function as:

$$\Lambda(\mathbf{r} \mid \mathbf{a}, \widetilde{\theta}, \widetilde{\tau}) = \exp\left\{ -\frac{1}{2\sigma_n^2} \sum_{k=0}^{NL_o-1} \left| r(k) - \sqrt{\frac{2E_s}{T}} \exp(j[\widetilde{\theta} + \varphi(\mathbf{a}; kT_s - \widetilde{\tau})]) \right|^2 \right\} \tag{2-4}$$

$\widetilde{\theta}$ and $\widetilde{\tau}$ in (2-4) represent the estimated values of θ and τ. Since, the exponential function is a monotonic function, one can take the natural log of both sides in the above equation and drop any constant multipliers. The likelihood equation becomes

$$\Lambda_1(\mathbf{r} \mid \mathbf{a}, \widetilde{\theta}, \widetilde{\tau}) = \sum_{k=0}^{NL_o-1} \left| r(k) - \sqrt{\frac{2E_s}{T}} \exp(j[\widetilde{\theta} + \varphi(\mathbf{a}; kT_s - \widetilde{\tau})] \right|^2 \qquad (2\text{-}5)$$

Minimizing equation (2-5) is equivalent to minimizing

$$\Lambda_1(\mathbf{r} \mid \mathbf{a}, \widetilde{\theta}, \widetilde{\tau}) = \sum_{k=0}^{NL_o-1} \left| r(k) - \sqrt{\frac{2E_s}{T}} \exp(j[\widetilde{\theta} + \varphi(\mathbf{a}; kT_s - \widetilde{\tau})] \right|^2 T_s \qquad (2\text{-}6)$$

Letting $T_s \rightarrow 0$ gives

$$\Lambda_2(\mathbf{r} \mid \mathbf{a}, \widetilde{\theta}, \widetilde{\tau}) = \int_0^{NT} \left| r(t) - \sqrt{\frac{2E_s}{T}} \exp(j[\widetilde{\theta} + \varphi(\mathbf{a}; t - \widetilde{\tau})] \right|^2 dt . \qquad (2\text{-}7)$$

Expanding the right hand side yields

$$\int_0^{NT} \left| r(t) - \sqrt{\frac{2E_s}{T}} \exp(j[\widetilde{\theta} + \varphi(\mathbf{a}; t - \widetilde{\tau})] \right|^2 dt =$$
$$\int_0^{NT} |r(t)|^2 dt + \int_0^{NT} \frac{2E_s}{T} dt - \int_0^{NT} 2\sqrt{\frac{2E_s}{T}} \operatorname{Re}\left\{ r(t) \exp(j[\widetilde{\theta} + \varphi(\mathbf{a}; t - \widetilde{\tau})]) \right\} dt \qquad (2\text{-}8)$$

The first two terms in equation (2-8) are not dependent on $\widetilde{\theta}$ and $\widetilde{\tau}$. Furthermore, they are independent of the data sequence. The likelihood equation can be written as follows:

$$\Lambda_3(\mathbf{r} \mid \mathbf{a}, \widetilde{\theta}, \widetilde{\tau}) = \int_0^{NT} \operatorname{Re}\left\{ r(t) s(\mathbf{a}, \widetilde{\theta}, t - \widetilde{\tau}) \right\} dt \qquad (2\text{-}9)$$

where,

$$s(\mathbf{a}, \widetilde{\theta}, t - \widetilde{\tau}) = \sqrt{\frac{2E_s}{T}} \exp(j[\widetilde{\theta} + \varphi(\mathbf{a}; t - \widetilde{\tau})] \qquad (2\text{-}10)$$

Since a negative constant −2 was dropped in obtaining equation (2-9), one needs

to find the data sequence of **a** that maximizes the likelihood function value, i.e., find

$$\widetilde{a} = \max_{\widetilde{a}} \int_0^{NT} \mathrm{Re}\{r(t)s(\mathbf{a}, \widetilde{\theta}, t - \widetilde{\tau})\} dt \qquad (2\text{-}11)$$

where, $\widetilde{a}$ is the data sequence which maximizes the above likelihood function.

According to equation (2-11) to recover the data sequence with a reliable accuracy, the

time and phase uncertainty should be estimated with reasonable accuracy prior to MLSD

symbol detection.

Computing the log-likelihood function for all possible **a** is not practical since the

possible number of sequences of **a** grows exponentially with its length. However, if the

signal has a trellis representation, then the Viterbi Algorithm can be used to simplify the

search.

Equation (2-9) can be rewritten as

$$L_c(\mathbf{a}_n, \widetilde{\theta}, \widetilde{\tau}) = \int_0^{NT} \mathrm{Re}\{r(t)s(\mathbf{a}, \widetilde{\theta}, t - \widetilde{\tau})\} dt = \sum_{n=0}^{N-1} BM_c(\mathbf{a}_n)$$

(2-12)

where

$$BM_c(\mathbf{a}_n) \equiv \int_{nT}^{(n+1)T} \mathrm{Re}\{r(t)s(\mathbf{a}, \widetilde{\theta}, t - \widetilde{\tau})\} dt \qquad (2\text{-}13)$$

$BM_c(\mathbf{a}_n)$ is a branch metric that can be used by the Viterbi Algorithm.

14

2.1.2 Trellis

As seen in Chapter 1 the CPM signal in the interval, $nT \le t < (n+1)T$ is determined by the phase function $\varphi(\mathbf{a}_n, t)$. It can be written as:

$$\varphi(\mathbf{a}_n, t) = \theta_n + 2\pi \sum_{i=n-L+1}^{n} h_i a_i q(t - iT) \qquad nT \le t < (n+1)T \qquad (2\text{-}14)$$

where, θ_n is

$$\theta_n = \pi \sum_{i=-\infty}^{n-L} h_i a_i \qquad (2\text{-}15)$$

Thus, in the n_{th} time interval the CPM signal is determined by

$$\alpha(n) = \{\theta_n ; a_{n-L+1}, ..., a_{n-2}, a_{n-1}\} \qquad (2\text{-}16)$$

and the current symbol a_n.

From the above calculations it can be concluded that a CPM scheme has a trellis representation if θ_n has a finite number of possible values. This is so if θ_n is created with a finite set of modulation indexes $\{h_0, h_1, ..., h_{H-1}\}$ which are all rational numbers [Weyi98]. Then, the number of trellis states is a fixed number

$$S = pM^{L-1} \qquad (2\text{-}17)$$

where p is obtained from the set of modulation indexes $\{q_0 / p, q_1 / p, ..., q_{H-1} / p\}$, p can be any positive integer as long as the greatest common divisor of the set $\{q_0, q_1, ..., q_{H-1}, p\}$ is 1.

A full response phase smoothing function with single-H with modulation index $\tfrac{1}{2}$ creates one of the simplest trellis representations. Figure 2.1 is an example of the phase trellis representation for binary full response scheme with h=1/2.
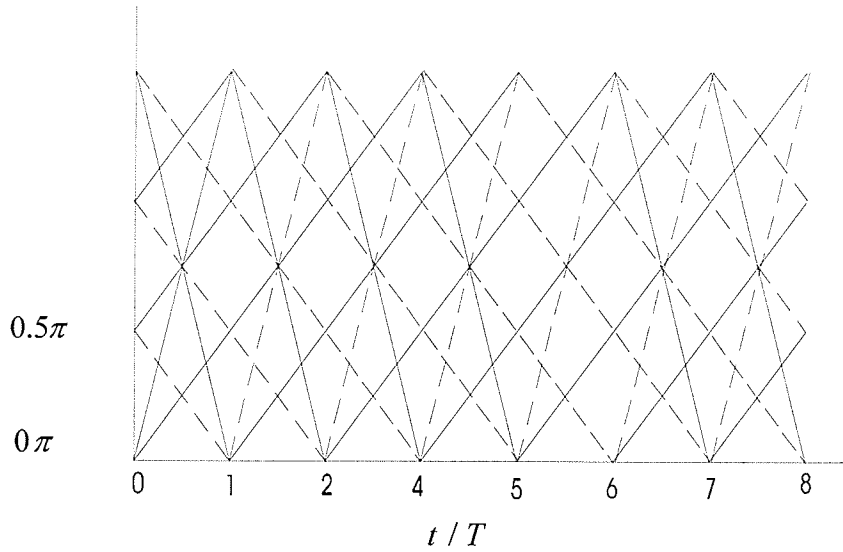
Figure 2.1 The phase trellis for binary full response scheme with h=1/2.

2.1.3 Optimum Receiver for CPM

The MLSD CPM receiver requires the computation of the branch metric, $BM_c(\mathbf{a}_n)$, in each symbol interval. By substituting equation (2-14) into equation (2-10), equation (2-13) can be rewritten as

$$BM_c(\mathbf{a}_L(n)) = \mathrm{Re}\{e^{j\bar{\theta}_n} \int_{nT}^{(n+1)T} r(t)h(\mathbf{a}_L(n),t)dt\} \qquad (2\text{-}18)$$

where, $\mathbf{a}_L(n) = (a_{n-L+1},...,a_{n-1},a_n)$ and

$$h(t,\mathbf{a}_L(n)) = \exp\left(j2\pi \sum_{i=n-L+1}^{n} h_i \tilde{a}_i q(t - \tilde{\tau} - iT) \right) \qquad (2\text{-}19)$$

There are M^L different functions $h(\mathbf{a}_L(n),t)$ for any n[th] interval. Denote this set of

$h(\mathbf{a}_L(n),t)$ possible functions as $\{h_1(t),\ h_2(t),\ \ldots,h_{M^L}(t)\}$. It follows directly from the

equation (2-18) that the most general form of the optimum MLSD receiver for CPM is as

shown in Figure 2.2.
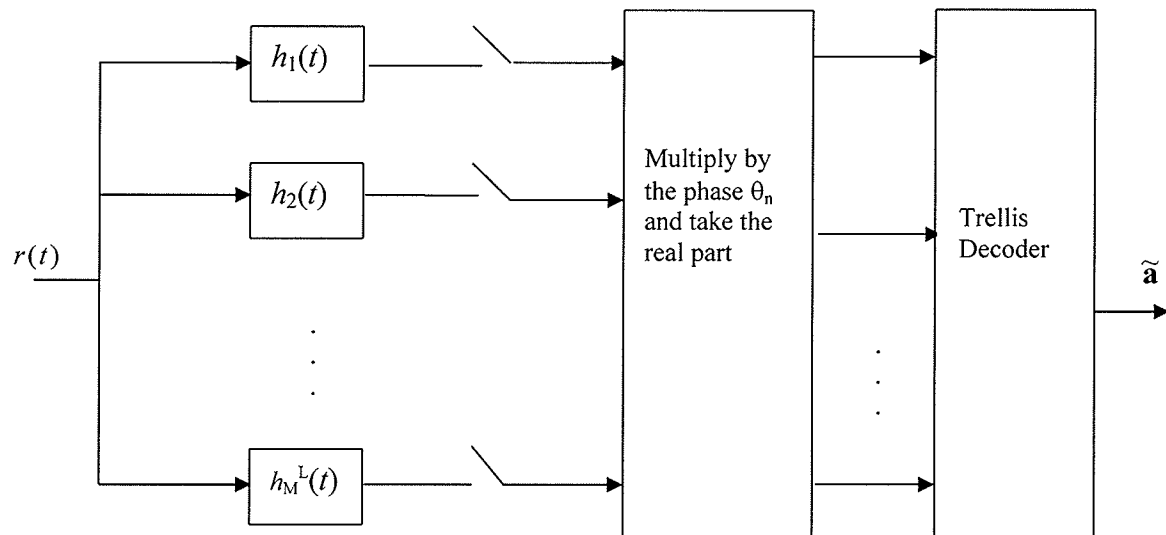
Figure 2.2 The optimum MLSD receiver.

It requires M^L complex matched filters followed by samplers which sample at

the end of each interval. To implement Figure 2.2 directly in practice, $4\,M^L$ filters are

required. However, since every sequence $\tilde{\mathbf{a}}_L$ has a corresponding sequence with a reverse

sign, only $2\,M^L$ matched filters are required. However this still can mean a fairly large

number of matched filters for partial response, M-ary CPM. For example, an optimum

receiver for quaternary, 3RC with $h = \frac{1}{2}$ requires 128 matched filters. Additional

difficulty exists for multi-H schemes. Equation (2-19) shows that the set $\{h(t,\tilde{\mathbf{a}}_L(n))\}$ is

different in different intervals for multi-H and there are H different sets of $\{h(t,\tilde{\mathbf{a}}_L(n))\}$ s

appearing cyclically. Thus, it is desirable to have a simpler sub-optimum receiver. The

next section discusses the sub-optimum receiver in signal space.

2.2 Receiver in signal space

Let $\{\eta_k(t), k = 0,1,...K-1\}$ be a subset of orthogonal basis functions of a complete

signal space for all the possible transmitted baseband signals $s(\widetilde{\theta}, t - \widetilde{\tau})$ when $t \in [0,T)$.

This space will be called the transmitter signal space and its basis functions are defined

over the time interval [0,T) and are zero outside this range. According to Parseval's

theorem the branch metric, $BM_c(\mathbf{a}_n, \widetilde{\theta}, \widetilde{\tau})$, of equation (2-13) can be expressed in terms

of $\{\eta_k(t)\}$ as:

$$BM_c(\mathbf{a}_n, \widetilde{\theta}, \widetilde{\tau}) = \sum_{k=0}^{K-1} \text{Re}\left\{ s_k^*(\widetilde{\theta}, t - \widetilde{\tau}) \int_{nT}^{(n+1)T} r(t)\eta_k(t - nT)dt \right\} \qquad (2\text{-}20)$$

where

$$s_k^*(\widetilde{\theta}, t - \widetilde{\tau}) = \int_{nT}^{(n+1)T} s(\widetilde{\theta}, t - \widetilde{\tau})\eta_k(t - nT)dt \qquad (2\text{-}21)$$

Though any basis set can be used, the set of Walsh Functions is particularly attractive due

to its simplicity. Let $w_k(t)$, $k = 0,1,...$, denote the Walsh Functions defined over the

time interval [0,T) where index k is expressed in the binary form as

$$k = \sum_{d=0}^{D-1} k_d 2^d \qquad (2\text{-}22)$$

$k_d \in \{0,1\}$ and $k_{D-1} \neq 0$. The Walsh functions are given by

$$w_k(t) = \begin{cases} \dfrac{1}{\sqrt{T}} \displaystyle\prod_{d=0}^{D-1} \text{sgn}\left(\cos\left(k_d 2^d \pi \dfrac{t}{T} \right) \right) & 0 \le t < T \\ 0 & \text{otherwise} \end{cases} \qquad (2\text{-}23)$$

where sgn(x) is defined as sgn(x)= 1, if $x \ge 0$, sgn(x)=-1 if $x<0$.

The first eight Walsh functions are shown in figure 2.3.
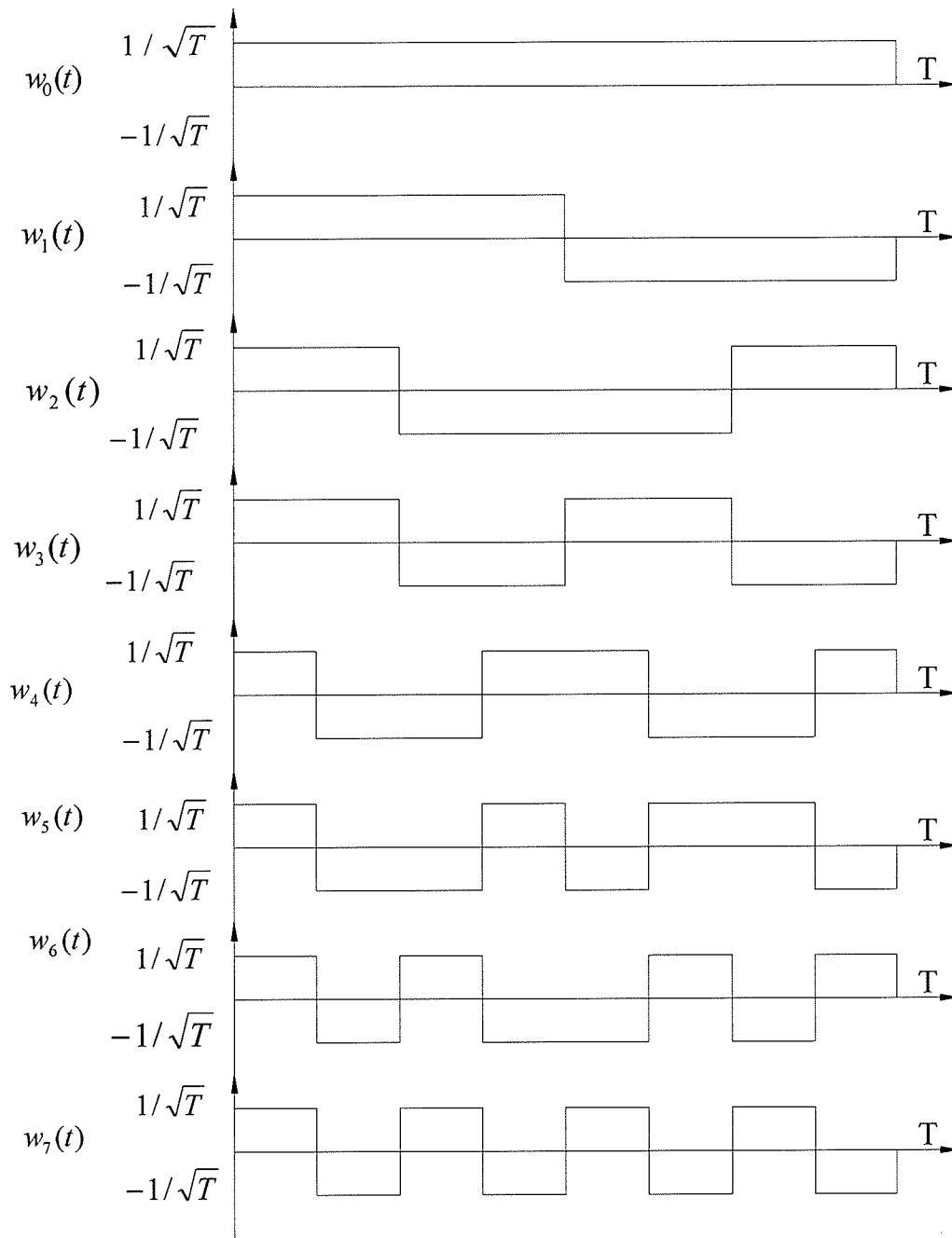
Figure 2.3 The first eight Walsh Function

Equation (2-21) becomes

$$s_k^*(\widetilde{\theta}, t - \widetilde{\tau}) = \int_{nT}^{(n+1)T} s(\widetilde{\theta}, t - \widetilde{\tau}) w_k(t - nT) dt \tag{2-24}$$

Consider the first K Walsh functions. The time interval [0,T] can be partitioned to K subintervals. From, equation (2-23) one can see that all the basis functions are constants $\pm 1/\sqrt{T}$. Let the subinterval be indexed by m=0,1,...,K-1 and denote the value of $w_k(t)$ in the mth subinterval $[mT/K, (m+1)T/K)$ as $w_k(m)$.

Then,

$$w_k(m) = \prod_{d=0}^{D-1} \text{sgn}\left(\cos\left(k_d 2^d \pi\left(\left(m+\frac{1}{2}\right)\frac{K}{T}\right)\right)\right)$$

(2-25)

where the coefficient $1/\sqrt{T}$ has been dropped.

The following tables show $w_k(m)$ for K=2 and 4 respectively.

Table 1. The value of $w_k(m)$ for K=2

m =	0	1
k = 0	1	1
k = 1	1	-1

Table 2. The value of $w_k(m)$ for K=4

m =	0	1	2	3
k = 0	1	1	1	1
k = 1	1	1	-1	-1
k = 2	1	-1	-1	1
k = 3	1	-1	1	-1

In Walsh Space the sufficient statistic $r_k(n) = \int_{nT}^{(n+1)T} r(t)\eta_k(t-nT)dt$ becomes.

$$r_k(n) = \sum_{m=0}^{K-1} w_k(m)\tilde{r}_m(n)$$

(2-26)

where,

$$\tilde{r}_m(n) = \int\limits_{nT+mT/K}^{nT+(m+1)T/K} r(t)dt \tag{2-27}$$

This shows that only two ordinary integrate-and-dump filters, followed by a sampler, which samples the output at a faster rate (K times faster), is required. The resulting structure is shown in Figure 2.4.
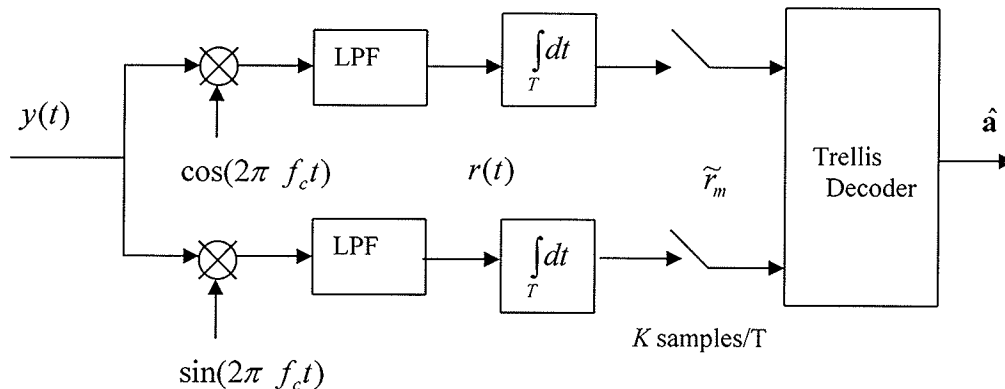
Figure 2.4 Structure of the sub-optimum receiver in Walsh signal space.

Simplicity is the most important benefit of the sub-optimum receiver in Walsh signal space shown in Figure2.4. This simplified receiver requires a reasonable synchronization. The next chapter is a discussion of synchronization techniques. Synchronization is especially important when the receiver is first turned on, which is known as acquisition. When the receiver is first turned on, the symbol timing and carrier phase difference between the receiver and received signal is usually too large for the receiver to detect the data sequence reliably and a linear assumption which would simplify synchronization is not valid. The next chapter focuses, in particular, on the acquisition process.

ACQUISITION

3.1 Introduction

Synchronization is a problem for all digital communication systems. It requires knowledge of four things: carrier frequency and carrier phase, symbol (or bit) frequency, and symbol timing. In most cases, the carrier frequency and symbol frequency are easily determined.

There are several methods of synchronization. One way to solve this problem is to send a reference signal separately from the modulated signal. But this solution wastes power and/or frequency spectrum. Besides, additive noise in the channel will cause a distortion in the signal making it undesirable to be used as a reference signal. When separate transmission is not feasible, the receiver usually must recover the symbol clock and carrier, from the received signal.

When the received signal is used, there are two approaches to synchronization – data-aided [HuLi92], [Tang98] and non-data aided [AnMM96], [MoMV97]. Data-aided synchronization is reasonable only if the data can be approximated with good accuracy or the data is known. In order to approximate the data with some accuracy, the symbol timing and the carrier phase uncertainty should be small: $\tau << T$ and $\theta << 2\pi$, typically

the error should be less than 10%. For this reason data-aided synchronization is a good approach for steady-state tracking. In tracking, only small changes to symbol timing and carrier phase, to combat slow drifts caused by additive noise, by channel and/or transmitter drift, are required. However, for acquisition, τ and θ are usually too large for reasonable data estimation. Thus, a non data-aided approach should be used or a known data sequence should be transmitted.

CPM is a very attractive modulation scheme but the extent of its future usage will be dependent on the receiver design and efficiency. Synchronization is a required step toward better CPM receiver designs. As discussed in Chapter 2, various CPM receivers have been designed. The Walsh signal space receiver developed by Tang [Tang98] is an improvement from previous receivers since it performs well with CPM signals with reasonable complexity. This receiver also provides for a reasonable implementation of synchronization, particularly in the tracking mode. The receiver performs well in steady-state tracking but not for acquisition, since a linear approximation is used in the synchronization.

The CPM signal is non-linear with respect to the symbol timing and carrier phase difference between the receiver and the received signal. Thus, a linear approximation is valid only over small interval segments of the parameters. In steady-state tracking, one assumes that symbol timing and carrier phase differences of the received signal and the receiver clock are relatively small ($\tau \ll T$ and $\theta \ll 2\pi$), whereas in acquisition, the clock offset, τ, can be comparable to a symbol period and the phase can be anywhere in the range of 0 to 2π.

Let us consider acquisition. For acquisition, using the non-data aided approach Andrea at al [AnMM96] suggest a joint carrier phase and symbol timing recovery by treating the data symbol and carrier phase as nuisance parameters. This method performs well, but the algorithm is complex and is difficult to implement.

Instead of approximating the data or treating it as a nuisance information, one could send a known sequence and utilize this information to stabilize the clock synchronization. Although sending a known sequence for acquisition purposes may waste power, it is justifiable for the overall robustness of system. It is common practice to use a pilot signal for the acquisition purpose, especially for those systems where the accurate time synchronization is demanded, such as in TDMA system [YuGe99]. Sending a known sequence is justified in terms of accuracy and speed of the acquisition.

The acquisition, proposed in this thesis, also uses a pilot signal. Using the pilot signal, one can estimate the symbol timing and carrier phase discrepancy between the receiver clock and the received signal in two steps. First, detect in which interval the parameters lie. As mentioned earlier, the linear approximation is only valid over a small interval. Thus, the interval size should be relatively small compared to T for symbol timing or to 2π for carrier phase. The exact interval size will vary with the signal types. Then, after detection of the interval, a linear approximation similar to the synchronization technique described by Tang is used.

After acquisition, the synchronizer works in the steady state where the only small changes, due to channel transmitter drift and channel noise, need to be estimated. Further, once acquisition is established, one can estimate the data sequence with reasonable accuracy to use it for the data-aided tracking.

This chapter presents general issues associated with symbol timing and carrier phase synchronization. The tracking method for small discrepancies in symbol timing and carrier phase is discussed first. Then, the acquisition method is presented.

3.2 Estimation

In baseband, the received signal with a complex envelope before synchronization can be written as

$$r(t) = s(t, \mathbf{a}, \tau, \theta) + n(t) = \sqrt{\frac{2E}{T}} e^{j\theta} e^{j\varphi(\mathbf{a}, t-\tau)} + n(t) \qquad (3\text{-}1)$$

where $n(t)$ denotes the baseband noise, θ is the phase difference between the carrier of the transmitted signal and the local oscillator of the receiver, and τ is the symbol timing difference between the transmitter and receiver. During the acquisition period, one cannot assume that θ and τ are bounded to a certain limit. However, for bit synchronization one only needs to find where the symbol boundaries are made. Thus the natural interval for symbol timing difference between the transmitter and receiver lies within the interval $-T/2 \le \tau < T/2$. The carrier phase difference between the carrier of the transmitted signal and the local oscillator is limited to $0 \le \theta < 2\pi$.

In the proposed acquisition method, one must detect in which interval the parameters lie first, and then using this information estimate the discrepancy between the symbol timing and carrier phase of the receiver and the received signal. However, the estimation method, where it is assumed that the discrepancy is small, is discussed first.

This section deals with estimation of the symbol timing and carrier phase differences between the received signal and the receiver when these differences are relatively small.

The correlation log-likelihood function (2-12) is now in the following form,

$$L_c(\theta, \tau) = \text{Re}\left\{ e^{-j(\theta)} \int_0^{NT} r(t) e^{-j\varphi(\mathbf{a}, t-\tau)} dt \right\} = \text{Re}\left\{ e^{-j\theta} Z(\mathbf{a}, \tau) \right\} \qquad (3\text{-}2)$$

where the data sequence, **a,** is assumed to be known

$$Z(\mathbf{a}, \tau) \equiv \int_0^{NT} r(t) e^{-j\varphi(\mathbf{a}, t-\tau)} dt \qquad (3\text{-}3)$$

One can either find a pair of $(\hat{\tau}, \hat{\theta})$ that maximizes the function (3-2) or average out one parameter and find the $\hat{\theta}$ or $\hat{\tau}$ which maximizes the function (3-2). According to equation (3-3) the phase uncertainty is independent of $Z(\mathbf{a}, \tau)$. Thus, the maximum likelihood estimate of the phase is simply

$$\theta = \arg\left[Z(\mathbf{a}, \tau) \right] \qquad (3\text{-}4)$$

$Z(\mathbf{a}, \tau)$ is relatively easy to find when the Walsh signal space approach is used, so τ is usually considered first.

The next subsections present two different methods of estimation. One can either assume that one variable is known and estimate the other variable or estimate both variables jointly.

3.2.1 Separate ML-estimation of Carrier Phase and Symbol Timing

One can assume that one of the variables is known and estimate the other variable. Although this is not a very practical assumption, it is a good way to illustrate ML-estimation principles. First, let's assume that τ is known.

To make equation (3-3) more manageable, one can approximate the mapping $\varphi(\mathbf{a}, t - \tau)$ by using a Maclaurin's series with respect to τ, an approximation that works well for small τ. Retaining only the first two terms of the mapping one has

$$\varphi(\mathbf{a}_n, t - \tau) \cong \varphi(\mathbf{a}_n, t) - \frac{\tau}{T} \psi(\mathbf{a}_n, t) \tag{3-5}$$

where,

$$\psi(\mathbf{a}_n, t) \equiv \frac{\pi}{L} \sum_{i=n-L+1}^{n} h_i a_i \mu(t - iT) \tag{3-6}$$

and,

$$\mu(t) \cong \begin{cases} 1 & \text{for REC} \\ 2\sin^2(\pi t / LT) & \text{for RC} \end{cases} \tag{3-7}$$

The details of the approximation are given in the Appendix.

Using equations (3-5), (3-6) and (3-7) one can approximate equation (3-3) by

$$Z_a(\mathbf{a}, \tau) \equiv \sum_{n=0}^{N-1} \int_{nT}^{(n+1)T} r(t) e^{-j\varphi(\mathbf{a}_n, t)} e^{j\frac{\tau}{T}\psi(\mathbf{a}_n, t)} dt \tag{3-8}$$

where $Z_a(\mathbf{a}, \tau) \cong Z(\mathbf{a}, \tau)$. Although, $Z_a(\mathbf{a}, \tau)$ is still difficult to evaluate it allows a further approximation as shown by the following equation:

$$e^{j\frac{\tau}{T}\psi(\mathbf{a}_n,t)} \cong 1 + j\frac{\tau}{T}\psi(\mathbf{a}_n,t) \tag{3-9}$$

This approximation is helpful to obtain an explicit solution for the estimation τ. The objective function, $Z_a(\mathbf{a},\tau)$, becomes

$$Z_a(\mathbf{a},\tau) \equiv \sum_{n=0}^{N-1} B(\mathbf{a}_n) + j\frac{\tau}{T}\sum_{n=0}^{N-1} C(\mathbf{a}_n) \tag{3-10}$$

where

$$B(\mathbf{a}_n) \equiv \int_{nT}^{(n+1)} r(t)e^{-j\varphi(\mathbf{a}_n,t)}dt \tag{3-11}$$

$$C(\mathbf{a}_n) \equiv \int_{nT}^{(n+1)} r(t)e^{-j\varphi(\mathbf{a}_n,t)}\psi(\mathbf{a}_n,t)dt \tag{3-12}$$

Clearly (3-10) is computable with the error caused by the approximation depending on the size of τ. Though $B(\mathbf{a}_n)$ and $C(\mathbf{a}_n)$ are still difficult to compute by a traditional approach, using the Walsh signal space approach enables the computation. According to (3-4) the phase is defined as $\arg(Z(\mathbf{a},\tau))$. Thus, using $Z_a(\mathbf{a},\tau)$ as an approximation for $Z(\mathbf{a},\tau)$ the phase can be approximated as,

$$\theta \cong \arg\left(B_s(\mathbf{a}) + j\frac{\tau}{T}C_s(\mathbf{a})\right) \tag{3-13}$$

where

$$B_s(\mathbf{a}) \equiv \sum_{n=0}^{N-1} B(\mathbf{a}_n) \tag{3-14}$$

$$C_s(\mathbf{a}) \equiv \sum_{n=0}^{N-1} C(\mathbf{a}_n) \tag{3-15}$$

Now, assume that the phase uncertainty is known. To determine the τ estimate, take the derivative of the correlation log-likelihood function (3-2). Setting it equal to zero yields,

$$\text{Re}\left\{e^{-j\theta}\frac{d}{d\tau}Z(\mathbf{a},\tau)\right\}=0 \tag{3-16}$$

Approximating $Z(\mathbf{a},\tau)$, using $Z_a(\mathbf{a},\tau)$, the derivative can be calculated as

$$\frac{d}{d\tau}Z(\mathbf{a},\tau)\cong\frac{d}{d\tau}Z_a(\mathbf{a},\tau)=j\frac{1}{T}\sum_{n=0}^{N-1}\int_{nT}^{(n+1)}r(t)e^{-\varphi(\mathbf{a}_n,t)}e^{\frac{\tau}{T}\psi(\mathbf{a}_n,t)}\psi(\mathbf{a}_n,t) \tag{3-17}$$

Approximating the equation (3-16) using (3-8) yields

$$\frac{d}{d\tau}Z_a(\mathbf{a},\tau)\cong j\frac{1}{T}\left[\sum_{n=0}^{N-1}C(\mathbf{a}_n)+j\frac{\tau}{T}\sum_{n=0}^{N-1}D(\mathbf{a}_n)\right] \tag{3-18}$$

where

$$D(\mathbf{a}_n)\equiv\int_{nT}^{(n+1)}r(t)e^{-j\varphi(\mathbf{a}_n,t)}\psi^2(\mathbf{a}_n,t)dt \tag{3-19}$$

It is important to note that the approximation becomes optimum when $\tau\to 0$.

Solving for $\dfrac{\tau}{T}$ yields

$$\frac{\tau}{T}\cong-\frac{\text{Im}\left\{e^{-j\theta}C_s(\mathbf{a})\right\}}{\text{Re}\left\{e^{-j\theta}D_s(\mathbf{a})\right\}} \tag{3-20}$$

where

$$D_s(\mathbf{a})\equiv\sum_{n=0}^{N-1}D(\mathbf{a}_n) \tag{3-21}$$

29

3.2.2 Joint Estimation

In a real situation, it is not reasonable to assume that one or the other variable is known, especially in the acquisition step where one cannot assume that error was initially limited to a small range. However, upon closer examination of the correlation log-likelihood function, one finds that the magnitude of the log-likelihood is solely dependent on $Z(\mathbf{a}, \tau)$. Since $Z(\mathbf{a}, \tau)$ is not a function of θ, the joint estimation of (τ, θ) can be found in two steps by finding τ which maximizes $|Z(\mathbf{a}, \tau)|$. Note that the τ which maximizes $|Z(\mathbf{a}, \tau)|^2 = Z^*(\mathbf{a}, \tau)Z(\mathbf{a}, \tau)$ will also maximize $|Z(\mathbf{a}, \tau)|$. Therefore, taking the derivative of $Z^*(\mathbf{a}, \tau)Z(\mathbf{a}, \tau)$ with respect to τ and setting it equal to zero yields.

$$Z(\mathbf{a}, \tau) \frac{dZ^*(\mathbf{a}, \tau)}{d\tau} + Z^*(\mathbf{a}, \tau) \frac{dZ(\mathbf{a}, \tau)}{dt} = 0 \qquad (3\text{-}22)$$

However, since the first and the second terms of (3-22) are complex conjugates, (3-22) is true if

$$\text{Re}\left\{ Z^*(\mathbf{a}, \tau) \frac{dZ(\mathbf{a}, \tau)}{dt} \right\} = 0 \qquad (3\text{-}23)$$

Again using the approximation $Z_a(\mathbf{a}, \tau) \cong Z(\mathbf{a}, \tau)$ and $\dfrac{d}{d\tau} Z_a(\mathbf{a}, \tau) \cong \dfrac{d}{d\tau} Z(\mathbf{a}, \tau)$,

(3-23) can be rewritten as following

$$\text{Re}\left\{ Z_a^*(\mathbf{a}, \tau) \frac{dZ_a(\mathbf{a}, \tau)}{dt} \right\} = 0 \qquad (3\text{-}24)$$

Substituting (3-10) and (3-17) into equation (3-24), one will have a quadratic function of $\dfrac{\tau}{T}$. However, it has been shown [Tang98] that for $\dfrac{\tau}{T} \ll 1$, further approximation will not

compromise the performance too much. One can further approximate the $e^{j\frac{\tau}{T}\psi(\mathbf{a}_n,t)}$ as 1

for $Z_a^*(\mathbf{a},\tau)$ while still using the approximation (3-11) for the second part. Thus, equation

(3-24) can be approximated as

$$\mathrm{Im}\left\{\left(\sum_{n=0}^{N-1}B(\mathbf{a}_n)\right)^*\left(\sum_{n=0}^{N-1}C(\mathbf{a}_n)+j\frac{\tau}{T}\sum_{n=0}^{N-1}D(\mathbf{a}_n)\right)\right\}=0 \qquad (3\text{-}25)$$

Solving for $\dfrac{\tau}{T}$ yields

$$\frac{\tau}{T}\cong-\frac{\mathrm{Im}\left\{B_s^*(\mathbf{a})C_s^*(\mathbf{a})\right\}}{\mathrm{Re}\left\{B_s^*(\mathbf{a})D_s^*(\mathbf{a})\right\}} \qquad (3\text{-}26)$$

Applying equation (3-4)

$$\theta\cong\arg\left(B_s(\mathbf{a})+j\frac{\tau}{T}C_s(\mathbf{a})\right) \qquad (3\text{-}27)$$

Each of the approximations made compromises to the accuracy of the estimation.

However, the purpose of these approximations is not to get the exact value of the

parameters, but to get a reasonable estimate in order to make the receiver function

efficiently.

3.3 Detection

The previous section discussed estimation of symbol timing and carrier phase estimation over a small interval. This section deals with how to bring the parameters into the estimation range.

For this thesis, a pilot signal, $x(t)$, is used during the acquisition period. The pilot signal used in this thesis is an antipodal signal. For an M-ary signal it will be $\{a,-a,a,-a,a,-a,a...\}$ where $a \in \{1,3,....,M\}$. For convenience, $a = 1$ is chosen. The antipodal signal has the maximum number of symbol transitions compared to other data sequences of the same length.

3.3.1 Preliminary Carrier Phase Estimation

When the antipodal pilot signal is used, the baseband phase function without noise is further restricted to $\theta_0 \le \varphi < a\pi h / 2 + \theta_0$ for single h. For binary signals with h=1/2 the phase function limit is $\theta_0 \le \varphi < \pi / 4 + \theta_0$. Thus, if the phase of the baseband CPM signal is restricted, then the estimation of $\hat{\theta}$ can simply be calculated as,

$$\hat{\theta} = \text{Tan}^{-1} \frac{E\{\text{Im}(r(t))\}}{E\{\text{Re}(r(t))\}} - E\{\arg(x(t))\} \tag{3-28}$$

where x(t) is the pilot signal and $E\{\arg(x(t))\}$ can be calculated and stored since one has prior knowledge of the pilot signal, $x(t)$. Phase uncertainty can be estimated without the knowledge of time uncertainty since the time uncertainty does not affect the average phase of the periodic signal. Also, attenuation does not affect the average phase.

Examine equations (1-6,1-7 and 1-8) again. The envelope is determined mostly by the carrier frequency since the carrier frequency is much higher than any phase change or instantaneous frequency change caused by the information bits. Thus, restricting the baseband phase will not affect the constant envelope feature of CPM.

3.3.2 Symbol Timing Detection

When the receiver is first turned on, the time uncertainty is not bounded to any time interval. Since the memory of the CPM serves as coding, it is important to find the time uncertainty beyond the natural symbol bound. The pilot signal here is dependent on the previous symbol only, so the time uncertainty interval becomes $-T \leq \tau < T$, which is larger than natural symbol bound, $-T/2 \leq \tau < T/2$, although it is still restricted.

To account for this the likelihood equation (2-12) should be examined from a different perspective; the unknown variable should be the symbol time and carrier phase difference between the receiver and the received signal, τ and θ.

The maximum likelihood estimate of τ and θ are then determined from the following likelihood equation.

$$\hat{\tau}, \hat{\theta} = \max_{\tau, \theta} \Lambda_4(r|\mathbf{a}, \tau, \theta) = \max_{\tau, \theta} \int_0^{NT} \mathrm{Re}\{r(t)s(\mathbf{a}, \theta, t - \tau)dt\} \qquad (3\text{-}29)$$

A straightforward approach to determine $\{\hat{\tau}, \hat{\theta}\}$ is to exhaustively evaluate $\Lambda_4(r|\mathbf{a}, \tau, \theta)$ over the range of $\{\tau, \theta\}$ values.

However, exhaustive evaluation is not practical. An alternative way to achieve this evaluation is to divide $[-T, T)$ into small intervals and detect in which interval the

symbol timing lies. Ideally, the maximum likelihood value of the equation (3-29) should

lie within the detected interval. Figure 3.1 shows how $[-T,T)$ can be divided into 2J

intervals. θ can be evaluated without using the likelihood equation as shown in the

previous section. The X marks the midpoints of the intervals. The midpoints of the

intervals represent approximate value of all the other points in the interval.
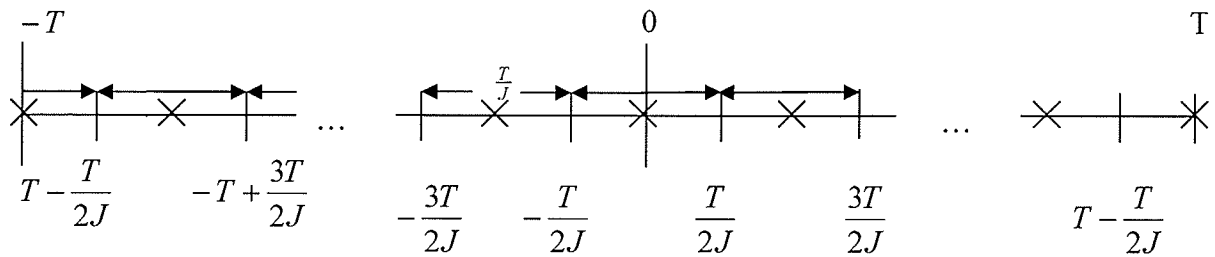
Figure 3.1 The subintervals

Accuracy of the estimation is largely dependent on interval size. Thus, the number

of intervals is determined by the maximum range over which the linear approximation is

reasonably justified and by how much error can be tolerated. The approximate value of

symbol timing is detected by testing the likelihood function (equation 3-29) with different

$\tilde{\tau}_i$ from the set of the midpoints of each interval,

$$\tilde{\tau}_i \in \left\{-T,...,\frac{-2}{J}T,\frac{-1}{J}T,0,\frac{1}{J}T,...,T-\frac{-1}{J}T\right\}. \; -T \text{ and } T \text{ is considered to be the same}$$

point since the pilot signal is antipodal.

Then,

$$\tau \approx \hat{\tau} = \max_{\tilde{\tau}_i} \Lambda_5(r|\mathbf{a},\tilde{\tau},\hat{\theta}) = \max_{\tilde{\tau}_i} \int_0^{NT} \text{Re}\left\{r(t)s(\mathbf{a},\hat{\theta},t-\tilde{\tau}_i)dt\right\}$$

$$(3\text{-}30)$$

where $i = -J,-J+1,...,0,1,2,3,...J-1$

Ideally, the true value of the symbol timing, τ, should lie in the detected interval,

$\left[-\dfrac{1}{2J}+\hat{\tau},\dfrac{1}{2J}+\hat{\tau}\right)$. Figure 3.2 represents the ideal situation. From the set of $\tilde{\tau}_i$ the

midpoint of the detected interval, $\hat{\tau}$, should be closest to τ.
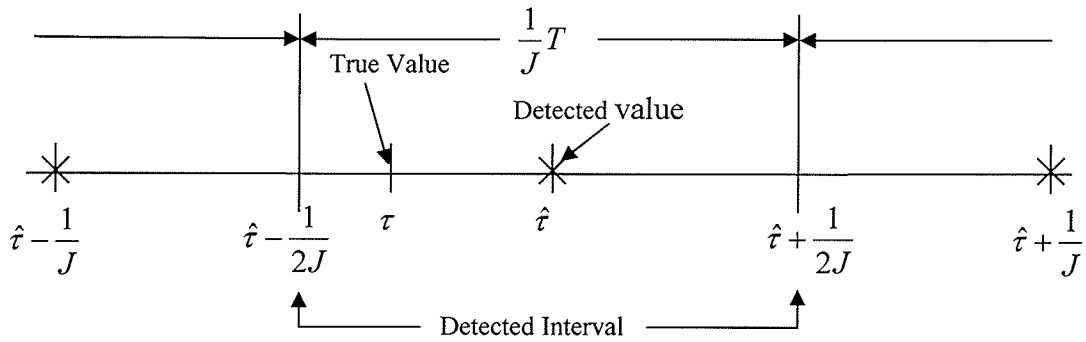
Figure 3.2 Detected Subinterval

If the true value of τ does not lie in the above interval, it is most probable to be in

the intervals adjacent to it, $[-\dfrac{1}{J}-\dfrac{1}{2J}+\hat{\tau},-\dfrac{1}{J}+\dfrac{1}{2J}+\hat{\tau})$ or $[\dfrac{1}{J}-\dfrac{1}{2J}+\hat{\tau},\dfrac{1}{J}+\dfrac{1}{2J}+\hat{\tau})$. If

the symbol timing does not lie in the detected interval or the intervals adjacent to it,

estimation based on linear approximation is likely to fail.

Unless J goes to infinity, there is an inherent error associated with detection. If

the τ lies in the detected interval and one assumes that the symbol timing lies with equal

probability anywhere in the interval (which possible only in noise free environment), then

the rms error of discrete detection is $\dfrac{T}{\sqrt{3}J}$, which implies that in general rms error of

discrete detection is greater than $\dfrac{T}{\sqrt{3}J}$. Hence, one needs to tighten the rms error margin

by estimation, using a linear approximation discussed in previous sections. The next

chapter will illustrate how the detection and estimation can be established in Walsh signal space.

IMPLEMENTATION AND PERFORMANCE

Acquisition is required when transmission begins. Acquisition is only an issue for a short period of time, but without successful acquisition the coherent receiver cannot function.

The last chapter discussed the need to differentiate between acquisition and steady-state tracking. The mathematical background of the steady-state tracking algorithm was discussed in detail and discretization of the parameters into intervals was introduced. Within each interval, a linear approximation can be used. Thus, one can estimate the symbol timing and carrier phase using a two-step approach in the acquisition stage. To find approximately where the symbol timing and carrier phase lie, one can divide the symbol time and phase range into finite intervals and detect which interval the parameters lie in. However, finding an approximate value of one parameter and detecting which interval the other parameter lies in with knowledge of the approximated parameter will reduce the computation significantly. Since the symbol timing and carrier phase have non-linear relationships with each other they cannot be completely decoupled. Nonetheless, one can approximate the carrier phase without the knowledge of the symbol timing if the pilot signal is chosen to restrict the carrier phase range. Using the approximate value of the carrier phase, the symbol timing range can be divided into finite

intervals. Then one can detect which interval the symbol timing lies in. After the interval is determined, one can further refine both the symbol timing and carrier phase estimate using a joint-estimation method. The joint-estimation method is also used in steady-state tracking stage.

This chapter discusses how the interval size and the length of training sequence are selected. Since it is intractable to obtain analytical solutions to the above questions, simulation is used to evaluate the acquisition algorithm.

4.1 Step One: Approximation

The first step for acquisition is approximation and there are two parts to this step: the initial phase approximation and symbol timing interval detection. This section discusses these parts of the approximation in detail.

4.1.1 Initial Phase Approximation

The carrier phase estimate can be made rather easily since the samples of the real and imaginary part of the signal are available from the sub-optimum receiver, which uses integrate-and-dump filters followed by samplers, in Walsh signal space (see Figure 2.4). The carrier phase of the received signal is the difference between the average phase of the received signal and average of the pilot signal phase.

It is also possible to obtain the carrier phase average by taking instantaneous samples without using the sub-optimum receiver, and taking the inverse tangent of the

real to imaginary signal ratio. Taking discrete samples introduces inherent error. Approximately 4 to 8 samples per bit for 2T where T is a bit interval for any periodic signal with period of 2T is sufficient to get the phase offset estimation limit below 15% when the signal is noise free. For a signal with additive noise, more frequent sampling of a longer sequence is required.

For the reasons discussed above, the first method of the carrier phase is more attractive and is the method chosen to be used in this thesis.

4.1.2 Symbol Timing Interval Detection

Once the phase estimate is obtained, symbol time estimation is considered. A major consideration is determining the appropriate interval size. The size should be selected so that the detected interval includes the received symbol timing most of the time. If the interval size is too large, the linear approximation for the second step is invalid. On the other hand, if the interval size is too small, the number of computations becomes intolerable. Thus, the interval size should be chosen to minimize the computations while still being able to use the linear approximation range.

To motivate and guide the selection of the interval size, consider a hypothetical probability density function of symbol timing shown in Figure 4.1. The symbol interval shown in Figure 4.1 represents the interval which has the highest probability of containing the true symbol timing. The interval selection is made using the midpoint of each interval. Thus, the midpoint of each interval is a target value and the one which is detected to be closest to the true symbol timing is denoted as $\hat{\tau}$. It is assumed that each

symbol bit T is divided into J intervals and the resulting interval size is $\dfrac{T}{J}$. If one

assumes that symbol timing is within $-T$ to T, then $2J$ different intervals should be

considered.

Probability Density of the True Symbol Timing
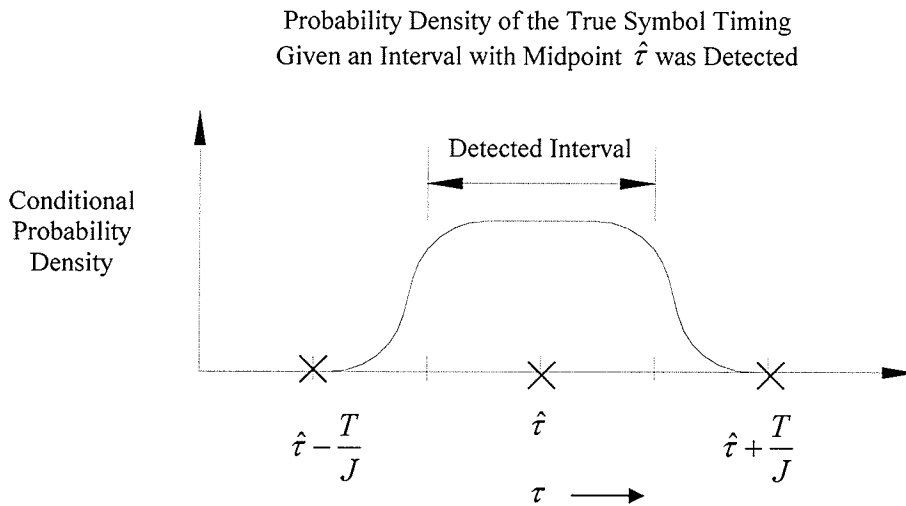Given an Interval with Midpoint $\hat{\tau}$ was Detected

Figure 4.1 Hypothetical Probability Density Function

Ideally the probability density function would be zero outside of detected interval.

It can have an arbitrary shape within the detected interval. Practically, additive noise will

affect the probability density function so that the symbol timing may lie outside the

detected interval. The goal of the detection is to detect a value which is close enough to

the true value to allow a linear approximation. It would be ideal if the true symbol timing

always was within $\dfrac{T}{J}$ away from the midpoint of the detected interval. According to W.

Tang's research [Tang98], the linear approximation is valid if the difference between the

detected value and the true value of symbol timing is within the range of 15 to 20% of the

symbol timing period, T. Thus, the interval size, $\dfrac{T}{J}$, should be less than 15 to 20% of T.

Now, look at how the likelihood function is evaluated at the target values.

To evaluate the likelihood function, one can write equation (3-30), with $\hat{\tau}$ as an argument, in Walsh signal space. Using the estimated phase $\hat{\theta}$.

$$\hat{\tau} = \max_{\tilde{\tau}} \int_0^{NT} \left\{ \text{Re}\{r(t)s(\mathbf{a}_n, \hat{\theta}, t - \tilde{\tau})dt \right\} \approx \max_{\tilde{\tau}} \sum_{n=0}^{N} B(a_n, \tilde{\tau}) \qquad (4\text{-}1)$$

where $\tilde{\tau}$ s are midpoints of the intervals which can be represented as

$$\tilde{\tau}_i \in \left\{ -T, ..., \frac{-2}{J}T, \frac{-1}{J}T, 0, \frac{1}{J}T, ..., T - \frac{-1}{J}T \right\} \text{ and the quantity } B(a_n, \tilde{\tau}) \text{ can be}$$

approximated in Walsh Signal space as

$$B(a_n, \tilde{\tau}) \approx \sum_{k=0}^{K-1} r_k(n) s_k^*(a_n, \tilde{\tau}) \qquad (4\text{-}2)$$

where

$$r_k(n) = \int_{nT}^{(n+1)T} r(t) w_k(t - nT) dt$$

$$\qquad (4\text{-}3)$$

$$s_k(a_n, \tilde{\tau}) = \int_{nT}^{(n+1)T} s(t - \tilde{\tau}) w_k(t - \tilde{\tau} - nT) dt$$

Since $r_k(n)$ is not a function of $\tilde{\tau}$, the receiver sampling does not need to be changed to accommodate the algorithm for the acquisition. However, one needs to obtain a $2J$ set of $s_k(a_n, \tilde{\tau})$ over the set of $\tilde{\tau}$'s in the range $-T$ to T. These values can be pre-calculated and stored in memory. Therefore, their computation does not tax the receiver hardware.

One of the ways to reduce the number of computations is to make J an integer multiple of K, the dimension of Walsh signal space, which was used to represent the received signal and pilot signal. This way, all the $s_k(a_n, \tilde{\tau})$'s with different $\tilde{\tau}$ will be very closely related to each other.

To examine how this could simplify the calculation, examine the case where $\tilde{\tau}$

and $\hat{\theta}$ are zero. Then equation (4-3) becomes

$$s_k(a_n) = \int_{nT}^{(n+1)T} e^{j\varphi(t,a_n)} w_k(t - nT) dt \tag{4-4}$$

Consider equation (4-4). It can be expressed by using the Walsh Function subinterval

defined in Equation (2-25) as

$$s_k(a_n) = \sum_{m=0}^{K-1} w_k(m) \widetilde{s}_m(a_n) \tag{4-5}$$

where

$$\widetilde{s}_m(a_n) = \int_{nT+mT/K}^{nT+(m+1)T/K} s(a_n) dt \tag{4-6}$$

By choosing J to be a multiple of K, $J = K \times I$, one can further subdivide the

Walsh function to J intervals which are associated with the Walsh Function subintervals.

Let the subinterval be indexed by $\beta = 0,1,2,...,J-1$ and denote the value of

$w_k(t)$ in the β th subinterval $[\beta T / J, (\beta+1)T / J)$ as $w_k(\beta)$. Then, $w_k(\beta) = w_k(m)$ for

$\beta = mI, mI+1,...,(m+1)I-2,(m+1)I-1$ when $m = 0,1,...,K-1$

The following tables show $w_k(\beta)$ for K=2 and 4 respectively.

Table 3. The value of $w_k(\beta)$ for K= 2.

m=	0	1
$\beta =$	$0,1,...,I-1$	$I,I+1,...,2I-1$
k=0	1	1
k=1	1	-1

Table 3. The value of $w_k(\beta)$ for K= 2.

m=	0	1	2	3
$\beta =$	$0,1,...,I-1$	$I,I+1,...,2I-1$	$2I,2I+1,...,3I-1$	$3I,3I+1,...,4I-1$
k=0	1	1	1	1
k=1	1	1	-1	-1
k=2	1	-1	-1	1
k=3	1	-1	1	-1

The equations (4-5) and (4-6) can be rewritten as

$$s_k(a_n) = \sum_{\beta=0}^{B-1} w_k(\beta)\widetilde{s}_\beta(a_n) \tag{4-7}$$

where

$$\widetilde{s}_\beta(a_n) = \int_{nT+\beta T/J}^{nT+(\beta+1)T/J} e^{j\varphi(t,a_n)} dt \tag{4-8}$$

The training sequence used in this thesis is an antipodal signal which has period 2T. Thus $s(a_n) = s(a_{n+2l})$, where l is an integer. It is interesting to note that $s(a_n)$ is symmetric to $s(a_{n-1})$ and $s(a_{n+1})$ with respect to their respective transitional points. Thus,

$$\widetilde{s}_{J-\beta}(a_{n-1}) = \widetilde{s}_\beta(a_n) \tag{4-9}$$

and

$$\widetilde{s}_{J-\beta}(a_{n-1}) = \widetilde{s}_{-\beta-1}(a_n) \tag{4-10}$$

Thus, there are only J values for the different $\widetilde{s}_\beta(a_{n-1})$'s for a given carrier phase approximation and $\widetilde{\tau} = 0$.

If $\widetilde{\tau} \neq 0$, one can index different $\widetilde{\tau}$'s as $\widetilde{\tau}(\alpha)$ where

$\alpha = -J, -J+1, -J+2, \ldots, 0, 1, \ldots J-1$, i.e. $\widetilde{\tau}(-J) = -T$, ..., $\widetilde{\tau}(-2) = \dfrac{-2}{J}T$, $\widetilde{\tau}(-1) = \dfrac{1}{J}T$,

$\widetilde{\tau}(0) = 0$, $\widetilde{\tau}(1) = \dfrac{1}{J}T$, $\widetilde{\tau}(2) = \dfrac{2}{J}T$, ..., $\widetilde{\tau}(J-1) = \dfrac{J-1}{J}T$ Then, the equation (4-4) can

be written as, (note: it is written with $\hat{\theta} = 0$ for simplicity sake, although the estimated $\hat{\theta}$

can be any other value)

$$s_k(a_n, \widetilde{\tau}(\alpha)) = \int_{nT}^{(n+1)T} e^{j\varphi(t-\widetilde{\tau}(\alpha), a_n)} w_k(t-nT) dt \tag{4-11}$$

where

$$s_k(a_n, \widetilde{\tau}(\alpha)) = \sum_{\beta=0}^{J-1} w_k(\beta) \widetilde{s}_\beta(a_n, \widetilde{\tau}(\alpha)) \tag{4-12}$$

$$\widetilde{s}_{\beta+\alpha}(a_n) = \widetilde{s}_\beta(a_n, \tau(\alpha)). \tag{4-13}$$

All $\widetilde{s}_\beta(a_n, \tau(\alpha))$'s are related to $\widetilde{s}_\beta(a_n)$ with $\widetilde{\tau} = 0$ by the following relationships.

When $\alpha \geq 0$

$$\widetilde{s}_{\beta+\alpha}(a_n) = \widetilde{s}_\beta(a_n, \tau(\alpha))$$
$$\text{If } \beta + \alpha \leq J-1$$

$$\widetilde{s}_{-(\beta+\alpha)}(a_n) = \widetilde{s}_\beta(a_n, \tau(\alpha))$$
$$\text{If } J-1 < \beta + \alpha \tag{4-14}$$

When $\alpha < 0$

$$\widetilde{s}_{\beta+\alpha}(a_n) = \widetilde{s}_\beta(a_n, \tau(\alpha))$$
$$\text{If } -J \leq \beta + \alpha$$

$$\widetilde{s}_{2J-1+\beta+\alpha}(a_n) = \widetilde{s}_\beta(a_n, \tau(\alpha))$$
$$\text{If } \beta + \alpha < -J$$

Thus, the likelihood function (4-1) can be evaluated if one has one set of $\tilde{s}_\beta(a_n)$'s with any value of $\tilde{\tau}$. The likelihood values with different $\tilde{\tau}$'s can be compared, and the maximum likelihood value $\hat{\tau}$ can be found.

4.2 Step Two: Fine Estimation

Once the interval that is most likely to contain the true symbol timing is chosen, one can use the joint estimation introduced in Chapter 3 to bring the estimated symbol timing and carrier phase closer to the true values.

Thus, consider how $C(a_n), D(a_n)$ (equation 3-12 and 3-19) can be calculated for the fine estimation. Now, $\tilde{\tau}(\alpha)$ represents a midpoint of an interval that is most likely to contain true symbol timing, $\hat{\tau}$.

$$C(a_n, \tilde{\tau}(\alpha)) \approx \sum_{k=0}^{K-1} r_k(n) u_k^*(a_n, \tilde{\tau}(\alpha)) \qquad (4\text{-}16)$$

$$D(a_n) \approx \sum_{k=0}^{K-1} r_k(n) v_k^*(a_n) \qquad (4\text{-}17)$$

where

$$u_k(a_n, \tilde{\tau}(\alpha)) = \int_{nT}^{(n+1)T} e^{j\varphi(t-\tilde{\tau}(\alpha), a_n)} \psi(t-\tilde{\tau}(\alpha), a_n) w_k(t-nT-\tilde{\tau}(\alpha)) dt \qquad (4\text{-}18)$$

$$v_k(a_n, \tilde{\tau}(\alpha)) = \int_{nT}^{(n+1)T} e^{j\varphi(t-\tilde{\tau}(\alpha), a_n)} \psi^2(t-\tilde{\tau}(\alpha), a_n) w_k(t-nT-\tilde{\tau}(\alpha)) dt. \qquad (4\text{-}19)$$

Similarly the equations (4-18) and (4-19) can be expressed as

$$u_k(a_n, \widetilde{\tau}(\alpha)) = \sum_{\beta=0}^{B-1} w_k(\beta) \widetilde{u}_\beta(a_n, \widetilde{\tau}(\alpha)) \tag{4-20}$$

$$v_k(a_n, \widetilde{\tau}(\alpha)) = \sum_{\beta=0}^{B-1} w_k(\beta) \widetilde{v}_\beta(a_n, \widetilde{\tau}(\alpha)) \tag{4-21}$$

$\widetilde{u}_\beta(a_n, \widetilde{\tau}(\alpha))$ and $\widetilde{v}_\beta(a_n, \widetilde{\tau}(\alpha))$ can be derived from the following equations,

$$\widetilde{u}_\beta(a_n) = \int_{nT+\beta T/K}^{nT+(\beta+1)T/K} e^{j\varphi(t,a_n)} \psi(t,a_n) dt \tag{4-22}$$

$$\widetilde{v}_\beta(a_n) = \int_{nT+\beta T/K}^{nT+(\beta+1)T/K} e^{j\varphi(t,a_n)} \psi^2(t,a_n) dt \tag{4-23}$$

where $\beta = 0,1,2,...,J-1$. Note that, $\widetilde{u}_{\beta+\alpha}(a_n, \tau(0))$ and $\widetilde{u}_\beta(a_n, \tau(\alpha))$ are related, as well as

$\widetilde{v}_{\beta+\alpha}(a_n, \tau(0))$ and $\widetilde{v}_\beta(a_n, \tau(\alpha))$ are related in the same way as $\widetilde{s}_{\beta+\alpha}(a_n, \tau(0))$ and

$\widetilde{s}_\beta(a_n, \tau(\alpha))$ are related in equation (4-14).

4.3 Simulation Results

Simulation is used to evaluate the two-step acquisition algorithm. To simulate acquisition algorithm performance, a received signal was created using a known data sequence and randomly selected symbol timing and carrier phase. The symbol timing was chosen to be equally likely within $-T$ to T and carrier phase was chosen to be equally likely within 0 to 2π. Thus, uniform pseudo random numbers between zero to one were scaled to be used as symbol timing and carrier phases for the received signal.

After the signal is generated, white Gaussian noise is added to simulate signal corruption from channel. The uniform random numbers were transformed using the Box-Muller algorithm to generate the Gaussian random numbers that can be used as white Gaussian noise. The Gaussian random numbers are then scaled with different scaling factors. The scaling factor decides the Signal to Noise Ratio (SNR). The SNR is

$$\frac{\text{Signal Power}}{\text{Noise Power} \times \text{Scaling Factor}}. \tag{4-24}$$

The first step to the simulation was to approximate the carrier phase and symbol timing. Carrier phase is approximated by comparing the average phase of the received signal and the average phase of the pilot signal. Next, one should determine in which interval the true symbol timing is most likely to lie. For interval detection, each bit is divided into eight subintervals. Thus, the subinterval size is $T/8$. It is divided into eight subintervals since $T/8$ is a small enough interval size for the symbol timing within that range to be expressed by a linear approximation. Next, the joint-estimation is used to bring the approximated symbol timing and carrier phase close to the true values.

A pilot signal is sent prior to transmission of data. The pilot signal itself does not convey any pertinent data but is simply used to aid the acquisition process. Thus, it is important to keep the pilot signal as short as possible. By studying the correlation of the pilot signal length with how closely one can approximate the unknowns, one can decide the ideal length of pilot signal.

This thesis focused on the acquisition-ability for 1RC, 2RC, 1REC and 2REC signals because they are the most commonly used CPM signals. The simulation code was written in C++.

4.3.1 The Carrier Phase Estimation

One of the indicators of acquisition algorithm performance is the RMS difference of the estimation value and true value.

Figure 4.2 shows the relationship between the RMS error of carrier phase estimation (difference between estimated carrier phase and true carrier phase) and the pilot signal length.
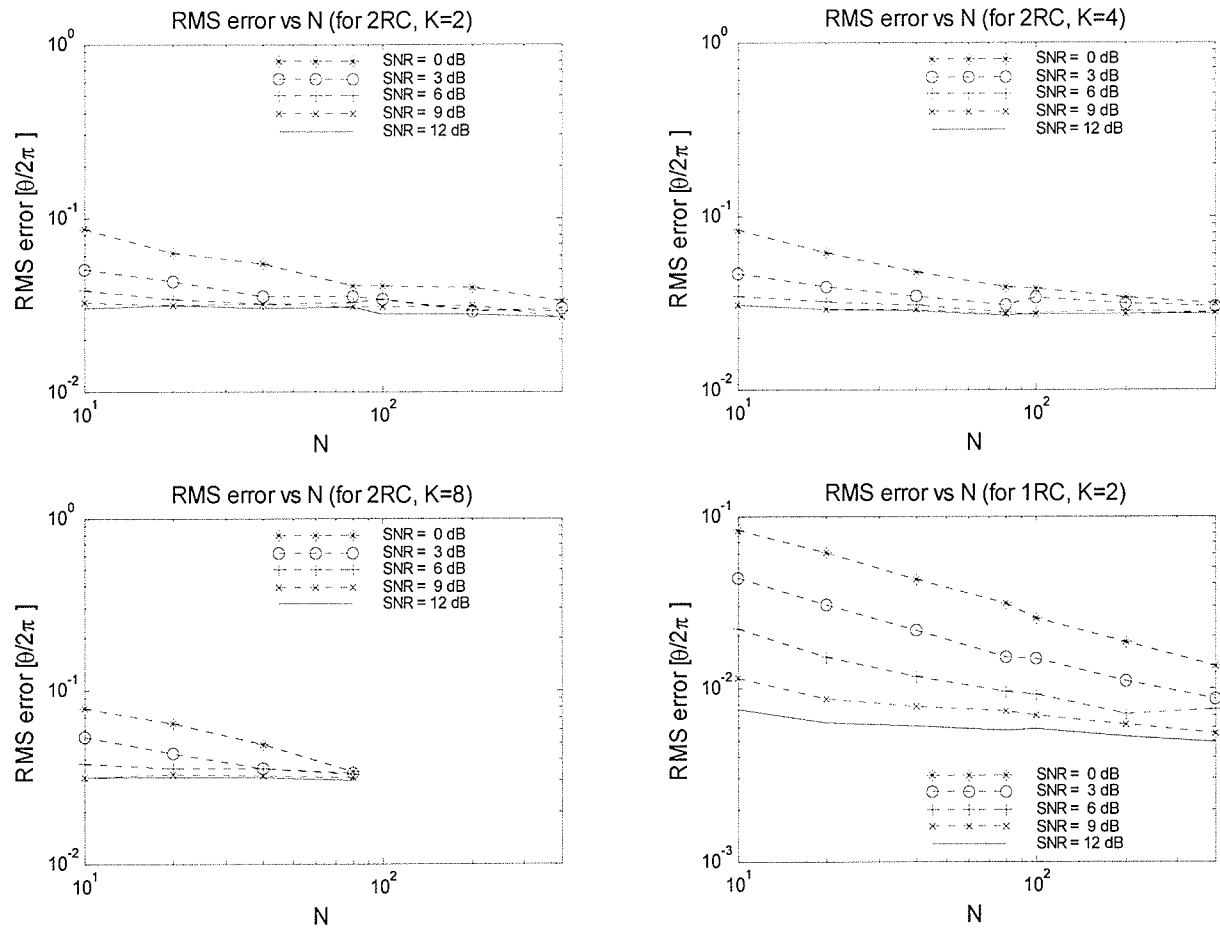
Figure 4.2 Difference between estimated carrier phase and true carrier phase of quaternary 2RC and 1RC with h=1/2, for different τ in 2 to 8 dimensional Walsh space for the pilot signal with different signal to noise ratio.

The above figure shows the simulated performance of multi-step acquisition algorithm that uses initial phase approximation, symbol timing subinterval detection and open-loop joint symbol timing and phase estimation for 2RC and 1RC, with h=1/2. The same pilot signal was used for both 1RC and 2RC. The simulation result appears to be better for the 1RC signal. This is due to the fact that the 1RC signal has larger phase change within a symbol period.

In all cases, the RMS difference of the estimated carrier phase and the true carrier phase is brought to less than 10% of 2π which is within the tracking range, for training sequence as short as 10 symbols.

The carrier phase estimation result for LREC scheme is not discussed here since the symbol estimation and carrier phase estimation are inter-related. Thus, having a good result for one would imply a good result for the other variable. Symbol timing estimation of LREC schemes is discussed in following sections.

4.3.2 The Symbol Timing Estimation

Now, let's examine the symbol timing estimation performance. When the estimated symbol timing and the true symbol timing difference is greater than 0.2T, one cannot guarantee reasonable steady state tracking. Thus, successful acquisition is achieved when both the symbol timing and carrier phase estimation are close enough to the true value to be in steady state tracking range. The RMS value difference of the estimated symbol timing and the true symbol timing is also a good indication of the algorithm performance.
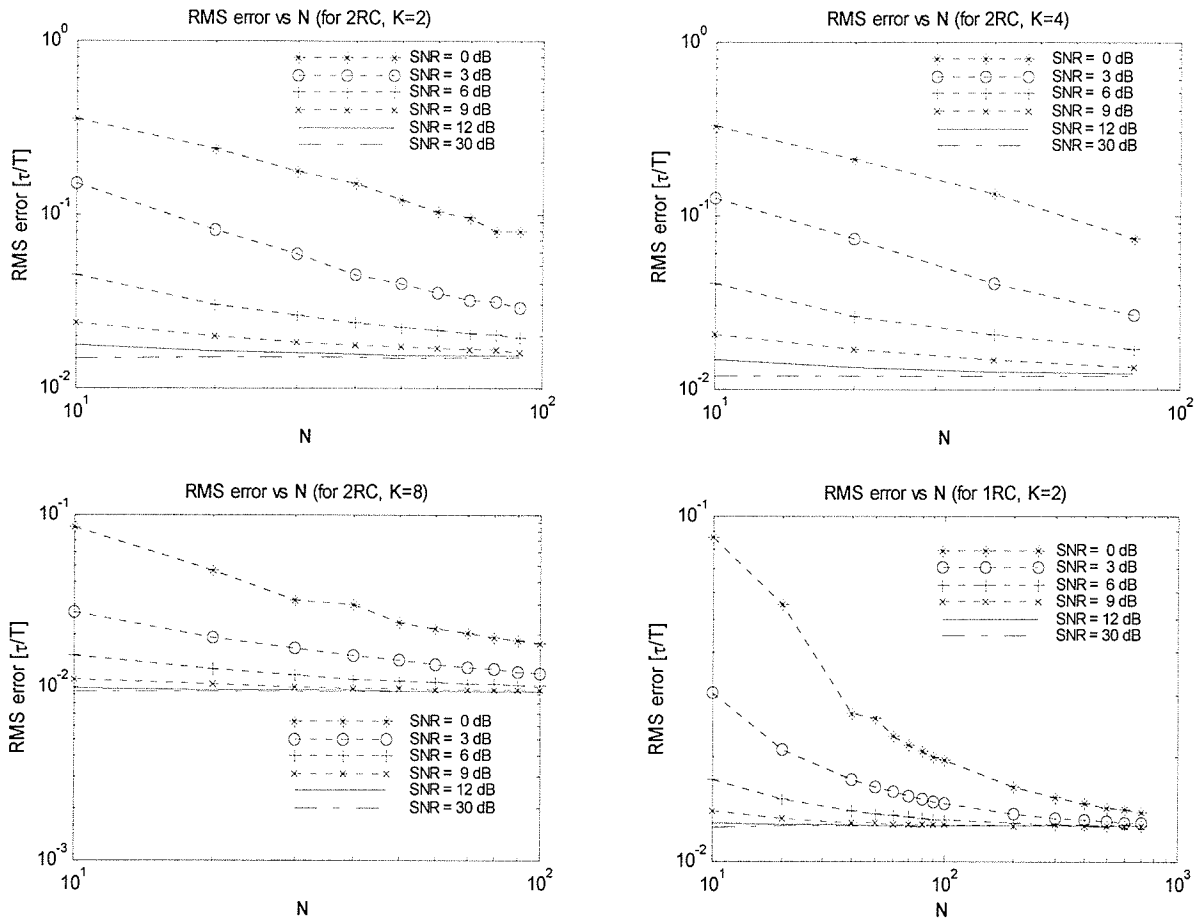
Figure 4.3 Difference between estimated symbol timing and true symbol timing of quaternary 2RC and 1RC with h=1/2, for different τ in 2 to 8 dimensional Walsh space for the pilot signal with different signal to noise ratio.

Figure 4.3 shows the relationship between the symbol timing RMS error

(difference between estimated symbol timing and true symbol timing) and the pilot signal

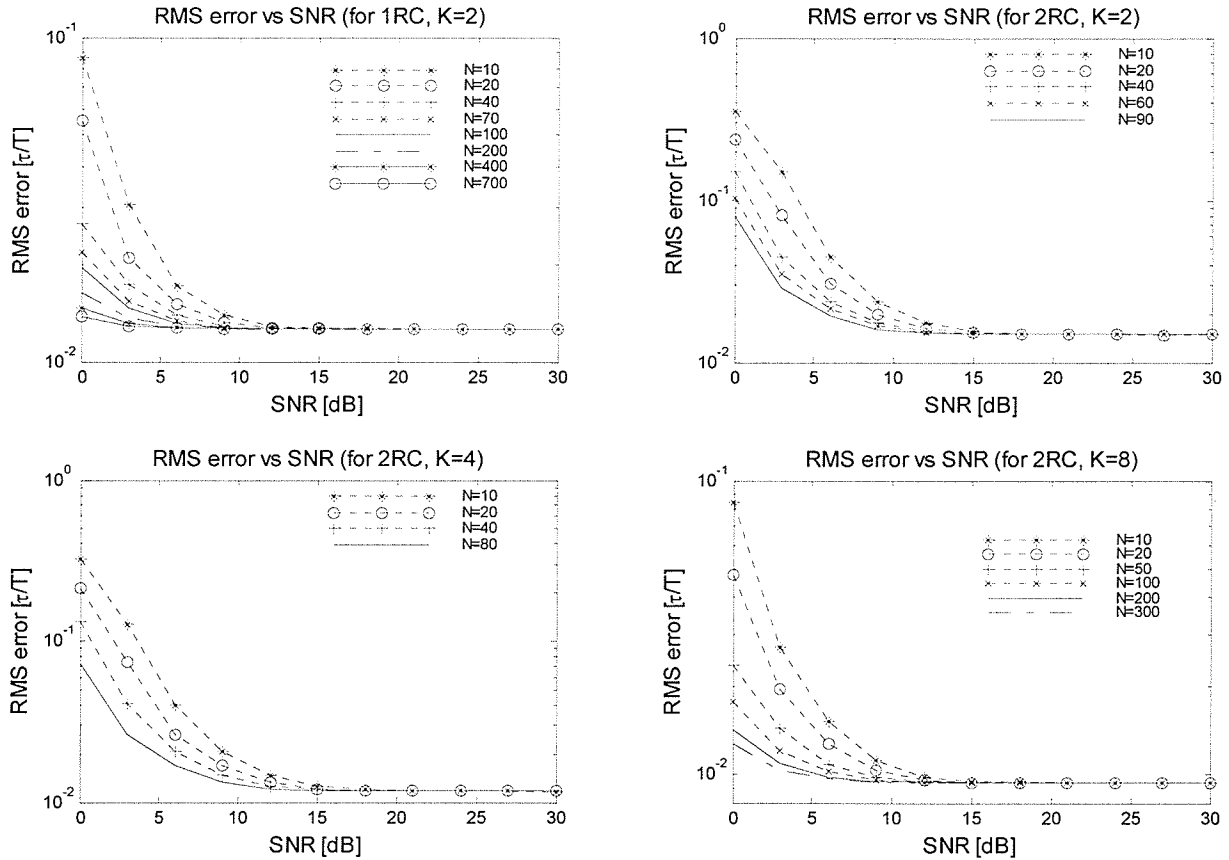length for 1RC and 2RC in 2 to 8 dimensional Walsh space for h=1/2

Figure 4.4 Timing error of quaternary 2RC and 1RC with h=1/2, for different τ in 2 to 8 dimensional Walsh space for the pilot signal with different signal length.

Figure 4.4 shows the timing estimation error vs SNR relationship for 1RC and

2RC in 2 to 8 dimensional Walsh space with h=1/2. Using Figure 4.3 and 4.4 one can see

that minimum length of pilot signal depends on the dimension of the Walsh signal space,

signal to noise ratio and the nature of the CPM. For many cases a pilot signal with length

N=10 is sufficient for the acquisition.

For SNR's greater than 15dB, Figure 4.4 shows that the performance for practical

purpose does not seem to be dependent on the length of training sequence. The

approximation error introduced to simplify the algorithm is greater than the effect of

noise or pilot signal length at that point.

4.3.3 The Symbol Timing Estimation in Different Walsh Signal Space Dimensions

In steady-state tracking, using a higher dimension of Walsh signal space does not seem to improve the performance significantly [Tang98]. This section examines how the acquisition performance behaves with Walsh signal space dimension.
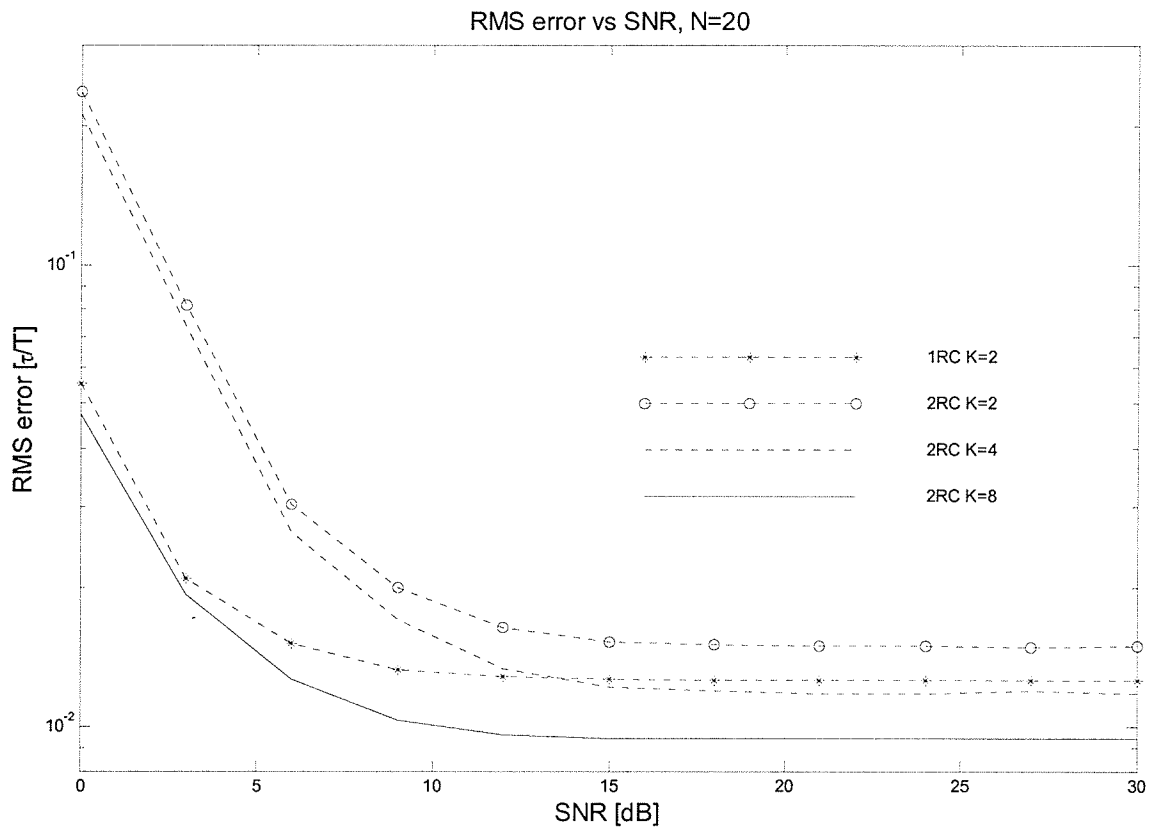

Figure 4.5 Comparison of timing error of quaternary 2RC and 1RC with h=1/2 in 2 to 8 dimensional Walsh space for the pilot signal with different signal to noise ratio.

Figure 4.5 more closely illustrates the relationship of the Walsh signal space dimension and the symbol timing estimation error. Unlike the randomized nature of the CPM, the pilot signal in CPM is very predictable. Also, the coding does not have any effect due to

the short length sequence and the nature of the training sequence. It is apparent that using

a higher dimension of Walsh signal space improves performance significantly when SNR
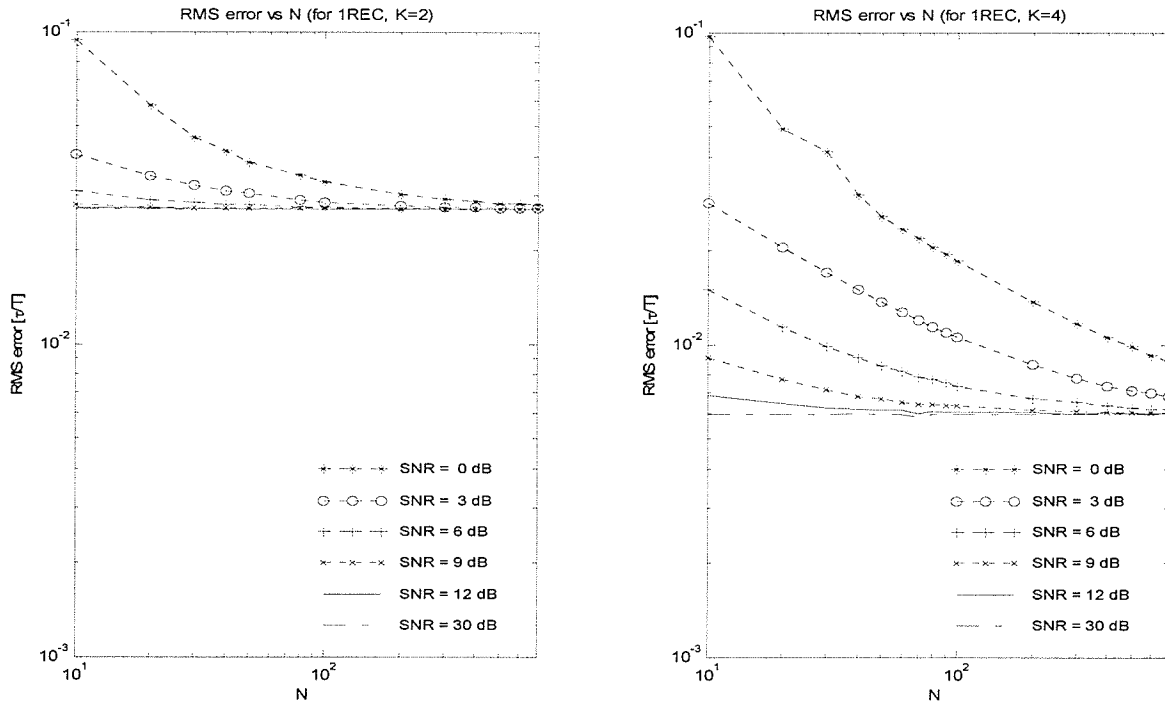
is low and the training sequence is short.

Figure 4.6 Timing error of quaternary 1REC with h=1/2, for different τ in 2 and 4dimensional Walsh space for the pilot signal with different signal to noise ratio.

Figure 4.6 and Figure 4.7 also show that using a higher dimension for the Walsh signal

space improves the performance for the 1REC signal. However, the improvement does

not seem to be as significant as for the RC signal at low SNR with a short training

sequence.

From the Figure 4.6, it can be observed that the relationship between performance

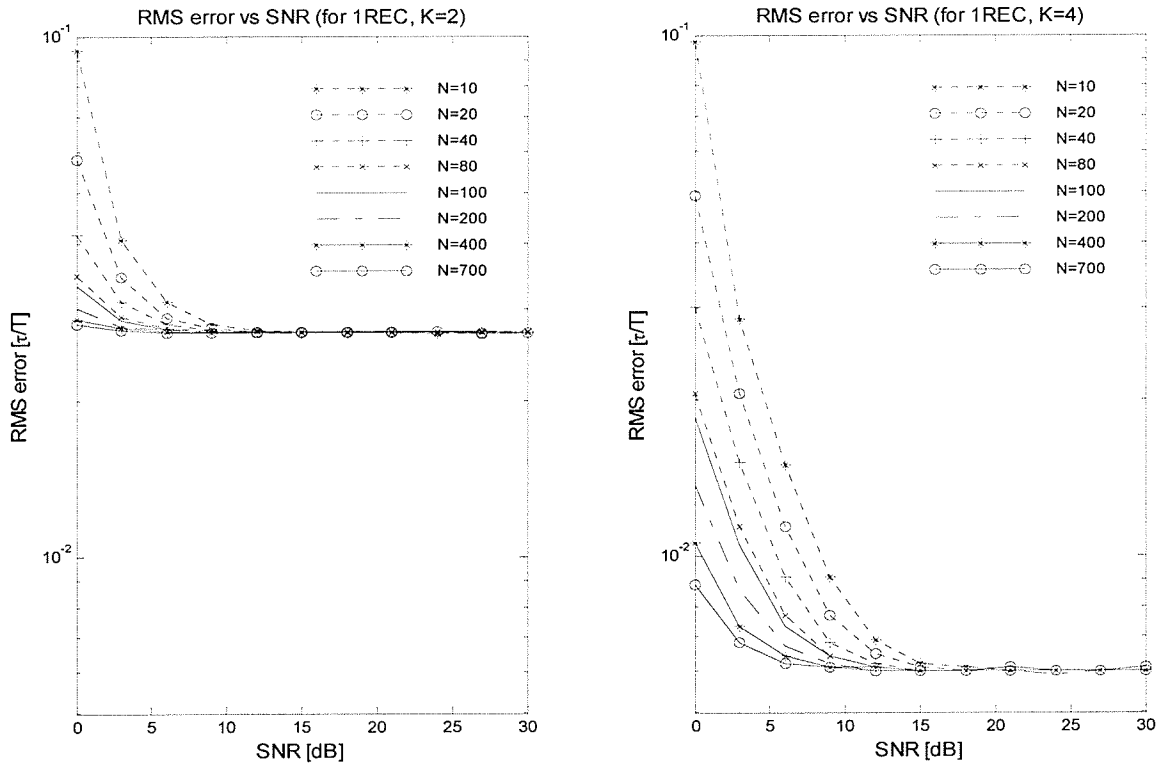improvement and training sequence length is not linear.

Figure 4.7 Timing error of quaternary 1REC with h=1/2, for different τ in 2 and 4 dimensional Walsh space for the pilot signal with different signal to noise ratio.

Figure 4.7 shows that for SNR greater than approximately 6 dB the symbol timing estimate will be within the tracking range of the true symbol timing. Thus, it would not be beneficial to increase the Walsh signal space dimension or training sequence length at high SNR.

4.3.4 Probability of Failure

RMS error is a good indicator of the acquisition algorithm performance. However, accuracy of the symbol timing and carrier phase estimate is not that critical an issue for this stage of synchronization. The acquisition only needs to bring the symbol timing and carrier phase estimate close enough for tracking purpose.

Figure 4.8 shows the frequency of the symbol timing estimate being 0 to 3%, 3 to 9%, 9 to 15%, and greater than 15% of T different from the true symbol timing.
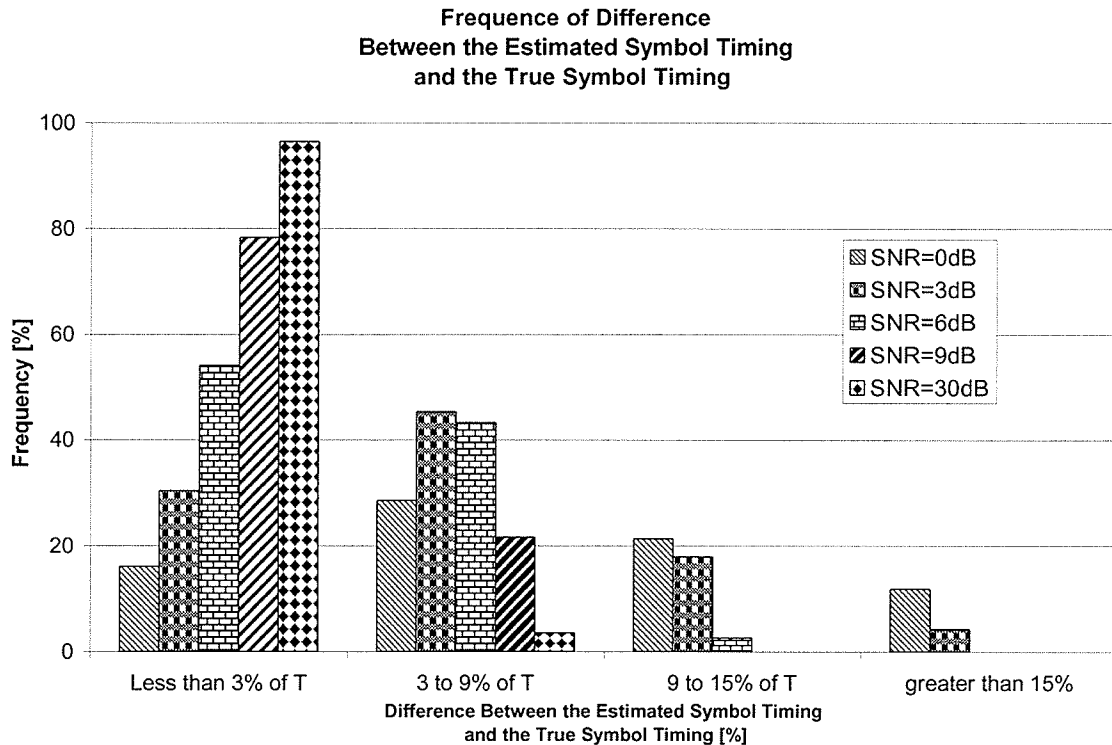
**Frequence of Difference
Between the Estimated Symbol Timing
and the True Symbol Timing**

Figure 4.8 Frequency of the symbol timing error of quaternary 2RC, N=20 with h=1/2, for different τ in 2 dimensional Walsh space for the pilot signal with different signal to noise ratio.

Figure 4.8 shows that for training sequence with SNR 6dB or greater is likely to bring the symbol timing estimate within the steady-state tracking range most of times. From the above histogram, it is most important to see what percentage of acquisition yields the symbol timing estimate greater than 15%.

One of the drawbacks of this algorithm is the fact that the algorithm cannot test whether the acquisition has been achieved in practice. With additive noise, perfect synchronization cannot be achieved in real life.

CONCLUSION AND SUGGESTIONS FOR FURTHER STUDY

5.1 Conclusion

The main attraction of using the CPM receiver in Walsh signal space is its simplicity. If the symbol timing and carrier phase difference between the receiver and received signal is small then also it can be effectively synchronized in the steady-state tracking mode.

The acquisition algorithm was designed with the goal of keeping the simplicity of the receiver and efficiency of the steady-state tracking ability. While this algorithm requires more computation than the steady-state tracking algorithm, there is no added hardware complexity. Since, the acquisition is only an issue for the short period of time when the receiver is turned on, this added complexity in algorithm may be justified. A relatively short training sequence is required for this algorithm, but it is justifiable for the overall robustness of the system especially when the received signal is corrupted with noise.

5.2 Suggestions for the further study

The performance of the acquisition algorithm was studied to determine the length of the required pilot signal. It would be interesting to study how it performs when, instead of applying one long pilot signal, one sends a shorter pilot signal multiple times and then estimates the symbol timing and carrier phase multiple times independently. The redundancy will allow one to reject those results which deviate significantly from the average result; also a reiteration method can be used. A disadvantage of repetition and reiteration would be added computation.

In the first step of the acquisition in this thesis phase was approximated. However, it would also be possible to come up with an algorithm to estimate the symbol timing first by determining where the transition lies. Also, one of the drawbacks to the algorithm that was presented in this thesis is the introduction of memory and the delay. Thus, real time estimation would be natural topic of further study.

The specified degree of error that could be tolerated was rather arbitrary. Perhaps future studies can relate tolerable error margin with symbol error performance.

THE MAPPING APPROXIMATION

One of the difficulties of estimating τ comes from the fact that its nonlinearity is hidden inside the mapping $\varphi(a, t - \tau)$ where $\bar{t} = t - \tau$. To avert this difficulty, the shaping function $q(t - \tau)$ in the interval $[\tau, LT + \tau)$ can be approximated by the first two terms of its Maclaurin's series with respect to τ. Then, the modified series can be extended in the time interval [0,LT) and the values outside the interval redefined. Examples of application to REC and RC schemes are given as following:

$$q(t - \tau) \cong \begin{cases} 0 & t < 0 \\ q(t) - \tau \dfrac{\mu(t)}{2LT} & 0 \leq t < LT \\ \dfrac{1}{2} & LT \leq t \end{cases} \qquad \text{(A-1)}$$

where,

$$\mu(t) \cong \begin{cases} 1 & \textit{for } \text{REC} \\ 2\sin^2(\pi\, t / LT) & \textit{for } \text{RC} \end{cases} \qquad \text{(A-2)}$$

Obviously, $|\tau| << T$. In equation (3-1), the time uncertainty τ is no longer hidden in nonlinearity but it stands out. For the REC scheme, it is exact except in the time interval $[0, \tau)$ and $[LT, LT + \tau)$ where $\tau > 0$, $[\tau, 0)$ and $[LT + \tau, LT)$ where $\tau < 0$. This approximation creates a discontinuity at 0 and LT for the REC scheme. However, this discontinuity does not affect the

continuity of the likelihood function, since the likelihood function is taken by integrating $Z(\mathbf{a}, \tau)$.

Figure A.1 shows examples of an above approximation.

Substituting (A-1) into equation (2-14) gives

$$\varphi(\mathbf{a}_n, t - \tau) = \varphi(\mathbf{a}_n, t) - \frac{\tau}{T} \psi(t, \mathbf{a}_n) \qquad \text{(A-3)}$$

where

$$\psi(\mathbf{a}_n, t) \equiv \frac{\pi}{L} \sum_{i=n-L+1}^{n} h_i a_i \mu(t - iT) \qquad \text{(A-4)}$$

Again, one can see from equation (A-3) that the approximation is exact in the time interval $[\tau, LT)$ when $\tau > 0$ or $[0, LT + \tau)$ when $\tau < 0$.
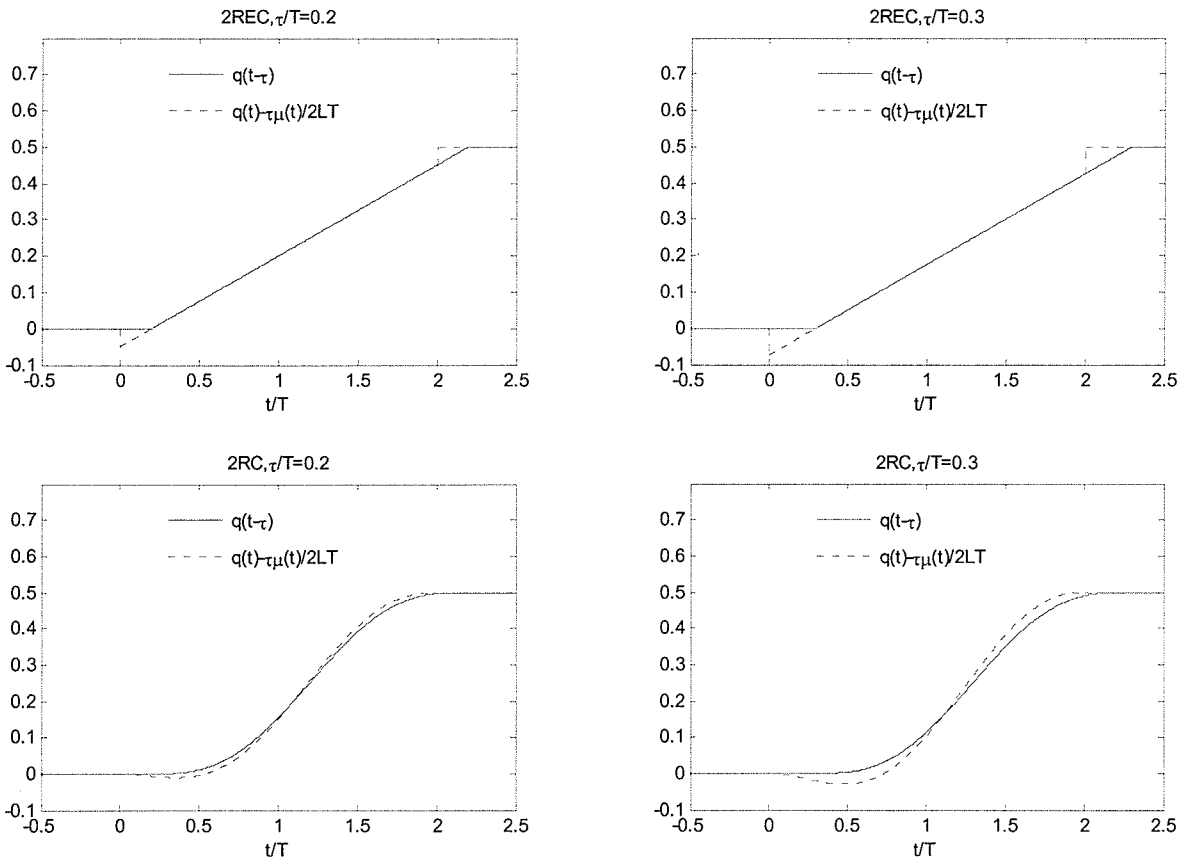

Figure A.1 Comparison between $q(t - \tau)$ **and its approximations for 2REC and 2RC,** $\tau / T = 0.2$ **and 0.3.**

This approximation not only makes it easier to take derivatives, but also it should be noted that $\varphi(\mathbf{a}_n, t)$ and $\psi(t, \mathbf{a}_n)$ can be calculated beforehand and stored as a known function of the receiver if the data sequence $\mathbf{a}_n$ is known.
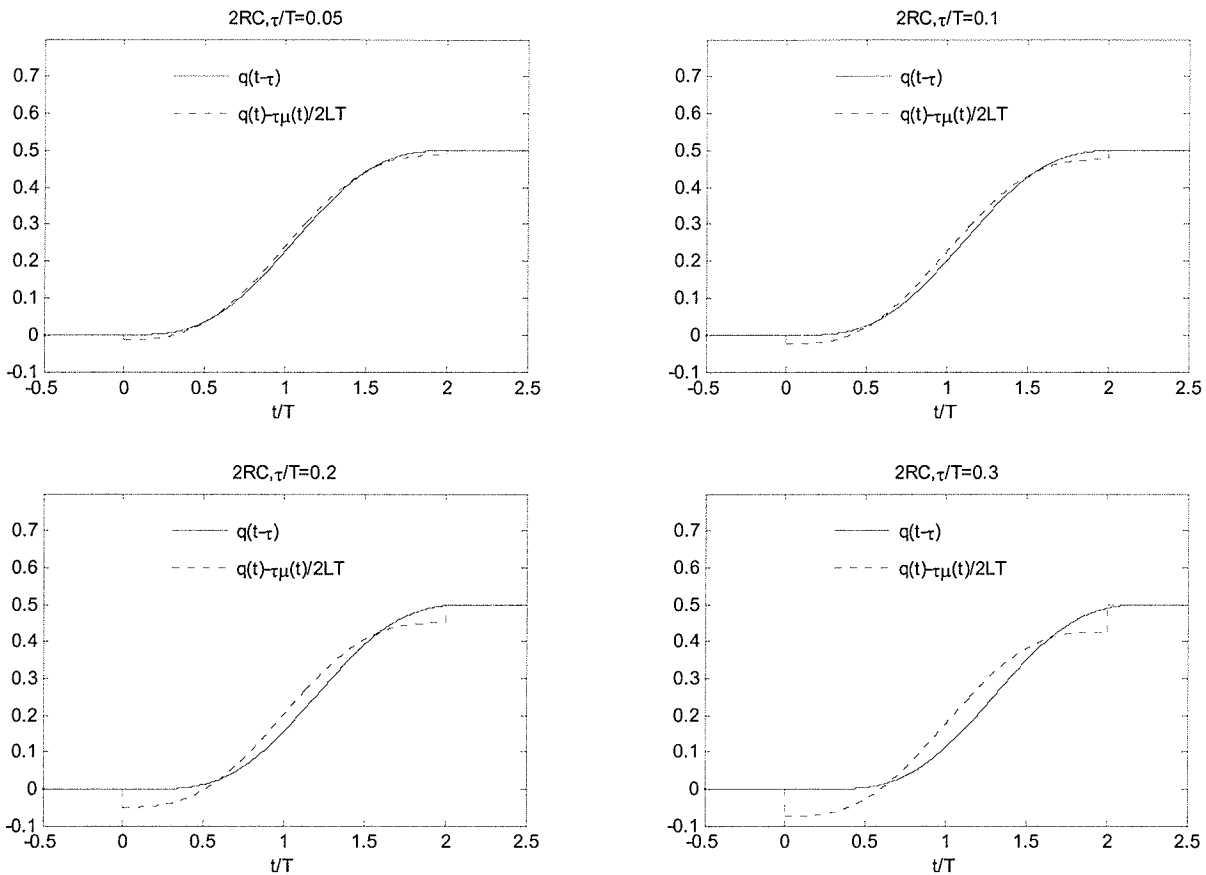

Figure A.2 Comparison between the phase pulse $q(t - \tau)$ **and its approximation** $q(t) - \tau\mu(t)/2LT$ **using** $\mu(t) = 1$.

It is also possible to use $\mu(t) = 1$ for RC scheme as well although it is a much poorer approximation. The Figure A.2 shows the comparison between exact $q(t - t)$ and its approximation $q(t) - \tau\mu(t)/2LT$ using $\mu(t) = 1$ instead of using $\mu(t = 2\sin^2(\pi \, t/LT)$. However, when τ is small, it still seems like fairly good approximation.

REFERENCES:

[AnAS86]   J. Anderson, T. Aulin and C. Sundburg, *Digital Phase Modulation*, Plenum

Press, New York, 1986.

[AnGM95]   A. Andrea, A. Ginesi and U. Mengali, "Frequency Detectors for CPM

Signals", *IEEE Transactions on Communications*, Volume 43, No.2/3/4,

Feb/Mar./Apr 1995

[AnMM96]   A. Andrea, U. Mengali and M. Morelli, "Symbol Timing Estimation with

CPM Modulation", *IEEE Transactions on Communication*, Volume 44, No

10, Oct 1996

[AnSv89]   S. Anderson and N. Svensson, "Noncoherent Detection of Convolutionally

Encoded Continuous Phase Modulation", *IEEE Journal on Selected Areas

in Communications*, Volume 7, No. 9, Dec 1989

[GiMM99]   A. Ginesi, U. Mengali and M. Morelli, "Symbol Timing Recovery in Multi-

H Continuous-Phase Modulation", *IEEE Transactions on Communications*,

Volume 47, No 5, May 1999

[HaKi89]   W. Harrold and N. Kingsbury, "Partially Coherent Detector for Continuous

Phase Modulation", *IEEE Journal on Selected Areas in Communications*,

Volume 7, No. 9, Dec 1989

[HuLi89]   J. Huber and W. Liu, "An Alternative Approach to Reduced-Complexity

CPM-Receivers", *IEEE Journal on Selected Areas in Communications*,

Volume 7, No. 9, Dec 1989

[HuLi92] J. Huber and W. Liu, "Data-Aided Synchronization of Coherent CPM-Receivers", *IEEE Transactions on Communications*, Volume 40, No. 1, Jan 1992

[HwLC89] H. Hwang, L. Lee and S. Chen, "Multi-*H* Phase-Coded Modulations with Asymmetric Modulation Indexes", *IEEE Journal on Selected Areas in Communications*, Volume 7, No. 9, Dec 1989

[Kale89] G. Kaleh, "Simple Coherent Receivers for Partial Response Continuous Phase Modulation", *IEEE Journal on Selected Areas in Communications*, Volume 7, No. 9, Dec 1989

[Kram92] G. Kram, *CPM Receiver Issues: The Matched Filter Bank and Sequential Sequence Estimation*, University of Manitoba Masters of Science Thesis, 1992

[KuSR89] S. Kuh, T. Strozier and C. Ryan, "Continuous Phase Quadrature Phase Shifted Keyed Signallying Technique with Coding", *IEEE Journal on Selected Areas in Communications*, Volume 7, No. 9, Dec 1989

[Laur86] P. Laurent, "Exact and Approximate Construction of Digital Phase Modulations by Superposition of Amplitude Modulated Pulses (AMP)", *IEEE Transactions on Communications*, Volume COM-34, No. 2, Apr 1986

[MeMo95] U. Mengali and M. Morelli, "Decomposition of M-ary CPM Signals into PAM Waveforms", *IEEE Transactions on Information Theory*, Volume 41, No. 5, Sep 1995

[MoMV97] M. Morelli, U. Mengali and G. Vitetta, "Joint Phase and Timing Recovery with CPM Signals", *IEEE Transactions on Communications*, Volume 45, No. 7 Jul 1997

[Seve91] A. Sevesson, "Reduced State Sequence Detection of Partial Response Continuous Phase Modulation", IEEE Proceedings-1, Volume 138, No.4, Aug 1991

[Sund86] C. Sundberg, "Continuous Phase Modulation", *IEEE Communications Magazine*, Volume 24, No., 4 Apr 1986

[Tang98] W. Tang, *A Receiver for Continuous Phase Modulation in Walsh Signal Space*, University of Manitoba Doctor of Philosophy thesis, Sep 1998

[YuGe99] W. Yuan and C. Georghiades, "Rapid Carrier Acquisition from Baud-Rate Samples", *IEEE Transactions on Communications*, Volume 47, No. 4 Apr 1999

[Xion94] F. Xiong, "Modem Technique in Satellite Communications", *IEEE Communications Magazine*, Aug 1994